Technical Report

424

Mutual Coupling in Array Antennas

J. L. Allen
B. L. Diamond

4 October 1966

Prepared for the Advanced Research Projects Agency
under Electronic Systems Division Contract AF 19(628)-5167 by

Lincoln Laboratory

MASSACHUSETTS INSTITUTE OF TECHNOLOGY

Lexington, Massachusetts

The work reported in this document was performed at Lincoln Laboratory, a center for research operated by Massachusetts Institute of Technology. This research is a part of Project DEFENDER, which is sponsored by the U.S. Advanced Research Projects Agency of the Department of Defense; it is supported by ARPA under Air Force Contract AF 19(628)-5167 (ARPA Order 498).

Distribution of this document is unlimited.

MASSACHUSETTS INSTITUTE OF TECHNOLOGY

LINCOLN LABORATORY

MUTUAL COUPLING IN ARRAY ANTENNAS

J. L. ALLEN

B. L. DIAMOND

Group 44

TECHNICAL REPORT 424

4 OCTOBER 1966

LEXINGTON MASSACHUSETTS

ABSTRACT

This report summarizes the current level of understanding of the performance of arrays of real radiators. The extent and nature of the effects of mutual coupling (element pattern distortion, element impedance variation with scan angle, and polarization variation with scan angle) in array antennas are investigated for a variety of array geometries and for several types of radiating elements. Both finite and infinite arrays of regularly spaced, uniformly illuminated, and progressively phased elements are considered. The effects of coupling on unequally spaced arrays, arrays with coupled feed networks, and circularly polarized arrays are also discussed. Finally, the results of a study of the effects of coupling on the radiation patterns of multiple-beam optical-type antennas are presented. Although most of the numerical results are based on thin, dipole radiating elements with and without ground planes (the dipole without a ground plane is the exact dual of an array of slots in a ground plane), both theoretical and experimental investigations of the sensitivity of the results to the element type are included. Emphasis is placed on the results of various analyses and their implications to the array designer. The derivations of some of the more important results are briefly outlined, but in most instances, only the relevant conclusions are given.

Accepted for the Air Force
Franklin C. Hudson
Chief, Lincoln Laboratory Office

CONTENTS

FOREWORD

The primary objective of this report is to provide the working engineer with a knowledge of the effects of mutual coupling on array performance – what the effects are and how serious they are. The theory and the necessary analytical tools for reproducing and extending the results are outlined and referenced, but the emphasis is on results; i.e., to what extent do the properties of an array depend on the kind of radiating elements used and the way they are excited?

The report thus has shortcomings that would be of interest to the well-rounded engineer: it ignores certain very fundamental results[1,2] that have not yet proven of practical value, and it ignores entirely the question of how to measure experimentally the effects discussed.[3-5] Although the purpose of this report is tutorial, many of the results are appearing here for the first time.

The origins of this report can be traced to 1961 when one of the authors prepared notes on array antenna theory for a summer course in "Elements of High Powered Radar Design" at M.I.T. In 1963, the revised notes were issued as a treatise on array theory.[6] At that time, the author was dissatisfied with the state of knowledge on mutual coupling; subsequently, both authors of the present report have devoted a great deal of time trying to improve the understanding of such phenomena. They were also fortunate to establish and maintain person-to-person communication with many others who have become interested in this area and whose names appear frequently in the references. As a result of these efforts, significant progress was made which thoroughly outdated the chapter on mutual coupling in Ref. 6 in just a few years.

The motivation for this updating of the authors' writings on mutual coupling research is due to Professor Curt Levis, Director of the Ohio State University Antenna Laboratory. At his invitation, the authors gave lectures during the summers of 1965 and 1966 as part of the University's curriculum on "Recent Advances in Antenna and Scattering Theory." The 1965 course notes formed the original draft for this report. For the 1966 course, the notes underwent a major revision. Since that time, only a few corrections have been made.

The authors are indebted to Professor Levis for the inspiration to write this report and for permission to publish it as a Lincoln Laboratory Technical Report. They are also appreciative of those who supported the work at Lincoln Laboratory, namely, the U.S. Air Force and, more recently, the Advanced Research Projects Agency. The authors especially thank Lt. Colonel John C. Toomay who was program director at ARPA and who has encouraged broad research of this type, insisting that the results be written in a manner intelligible to those not specializing in the field.

It would be impossible to list all those whose research contributed to the body of knowledge described in this report. The references do this to some extent, but do not give credit to the engineer whose experimental work is not published in the open literature. In this category, the authors especially acknowledge the contributions of L. Schwartzmann of Sperry Gyroscope Company and R. Tang of Hughes Aircraft Company whose observations and experiments have been helpful in verifying and extending the theory of mutual coupling effects.

For the interested reader, the authors recommend Microwave Scanning Antennas – Vol. II: Array Theory and Practice, R. C. Hansen, editor (Academic Press, New York, 1966). Chapters 2 through 4 by A. A. Oliner and R. G. Malech cover much the same material as this report but from a somewhat different viewpoint in some cases.

MUTUAL COUPLING IN ARRAY ANTENNAS

I. INTRODUCTION

A. Qualitative Explanation of Coupling Effects

It is intrinsic to the nature of antennas that when two antennas are in proximity and one is transmitting, the second will receive some of the transmitted energy, with the amount dependent on their separation and relative orientation. Even if both antennas are transmitting, they will simultaneously receive part of each other's transmitted energy. Furthermore, antennas rescatter a portion of any incident wave and thus act like small transmitters even when they are nominally only receiving. The result is that energy interchange between a particular element of an array and a remote point occurs not only by the direct path, but also indirectly via scattering from the other antennas of the array. This effect is a manifestation of the "mutual coupling" that exists between array antennas. It is not usually a negligible effect and complicates the design of such antennas.

Before attempting a quantitative examination of coupling effects, let us elaborate on the foregoing physical picture by examining (1) elements of a transmitting array and (2) elements of a receiving array (which may, in fact, be the same array at a different time).

1. Coupling in Transmitting Arrays

Imagine the two antennas shown in Fig. 1 as being two of many in an array. The generator attached to antenna n sets up a wave traveling from the generator toward the antenna indicated by the arrow labeled (0) in the figure. Part of this energy is radiated directly into space (1), while a part is coupled to the other antennas of the array – in this particular case, to antenna m. The field incident upon antenna m causes current flow in that antenna which reradiates some of the received energy (3) and also launches a wave toward the generator of antenna m (4). Of the energy rescattered (3), some is reradiated directly into space and some in turn couples again to other elements, and so forth. If antenna m is also being excited by its own generator, the energy rescattered from antenna m due to the generator excitation of antenna n adds vectorially to the energy from generator m, altering the amplitude and phase of apparent excitation of antenna m in a manner dependent on the output of generator n.

> Thus, the total contribution to the far-field pattern of a particular element in the array depends not only on the excitation furnished by its own generator (the direct excitation), but also on the total parasitic excitation, which depends on the couplings from and the excitation of the other generators.

The wave which is traveling toward the generator (4) of antenna m adds to any reflection from that antenna because of mismatch between the generator and the antenna. For the case of

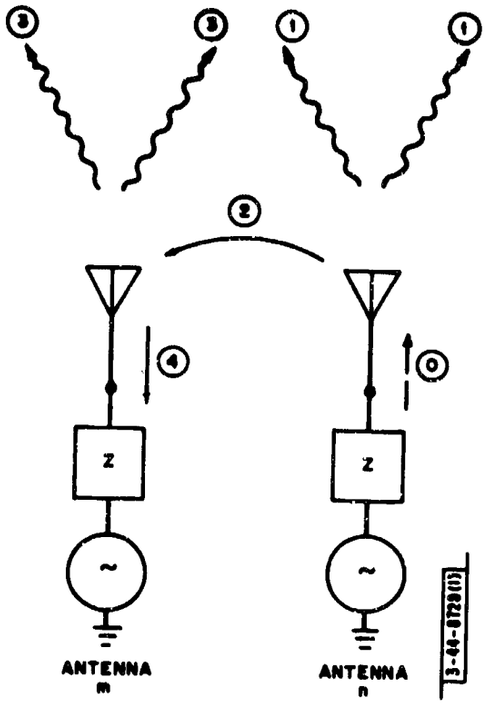

Fig. 1. Coupling paths from antenna n to antenna m when transmitting.

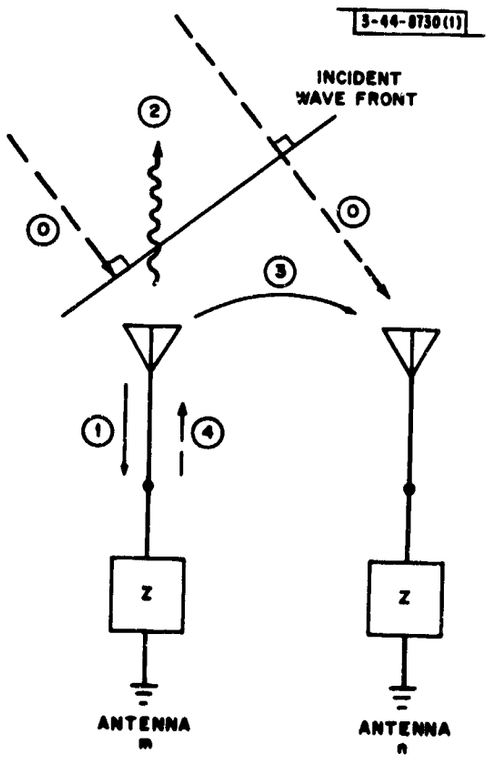

Fig. 2. Coupling paths from antenna m to antenna n when receiving.

principal interest here, in which the element excitations are coherent, the wave (4) due to generator n differs from the reflected wave in antenna m because of its own generator mismatch only in phase and amplitude; exactly how depends on the coupling between the two antennas and the complex amplitude of the output of generator n. The net effect of the vector sum of these two waves to an observer looking at antenna m from its generator is the same as if the impedance of antenna m were changing as a function of the excitation and location of antenna n. In fact, it is common practice to model this effect of coupling on such arrays as a change in the apparent driving impedance of the elements (this change is often termed the "mutual impedance variation").

While not entirely without its confusing aspects, the concept of a changing driving impedance is useful. For example, for a particular set of element excitations and locations in an array, the generator impedance that is optimum for each element (in the sense of maximizing the radiated power) would be a "match" to an impedance at the antenna terminals that would set up a reflected wave numerically equal in phase and amplitude to the backward traveling waves induced because of the coupling. Such a generator achieves maximum power transfer in an array, even though it is not the impedance which is a match to what one would measure looking into a single antenna without the other antennas excited.† Since the coupled waves depend on the excitation as well as the placement of the other antennas, the impedance selected is optimum only for that set of conditions. Thus we arrive at one of the principal aggravations of coupling in arrays whose element excitations are varied (such as in electronic scanning arrays):

> The generator impedance that would maximize the array radiation efficiency (gain) varies with the array excitation.

2. Coupling in Receiving Arrays

Figure 2 illustrates the coupling paths for a receiving array in which the receivers are represented as passive loads. Again, the figure depicts two elements of a large number assumed to be present in an array.

Assume that there is a plane wave incident as indicated by the arrows labeled (0) from a direction such that the incident wave will strike antenna m first. The field incident on antenna m causes current to flow on this antenna which launches a wave into its feed (1) and also rescatters some of the energy into space (2) and into adjacent antennas (3). The rescattered wave from antenna m (3) adds vectorially at antenna n to the wave directly incident from space.

---

† In order to minimize confusion, we adopt the following terminology:

(a) Antenna impedance: the impedance looking into a single isolated element.

(b) Passive driving impedance: the impedance looking into an element of an array with all other elements in place and passively terminated (in their normal generator internal impedances, unless otherwise specified).

(c) Active driving impedance: the impedance looking into an element of an array with all other antennas in place and excited (excitation must be specified).

Since impedance (b) is of minor importance and in most practical cases differs only slightly from (a), the term "driving impedance" alone will be understood to refer to the active driving impedance.

> Thus the total input energy to each antenna from the incident wave is the vector sum of the waves coming in directly from space as well as those coupled parasitically from the other antennas: it is dependent on the relative location of all the elements in the array.

Since the relative amount of energy absorbed and energy reradiated from any antenna depends on its match to its terminating impedance, the total input energy to each antenna depends on the terminating impedances of all the other antennas. In fact, for maximum extraction of energy from the passing wave, we would like to choose the terminating impedance of the elements in such a manner that we minimize the total energy backscattered into space (2). Consequently, we should actually mismatch the receiver relative to the antenna impedance in order to set up a reflection from the receiver back to the antenna (4) to cancel the wave that would have been rescattered had the receiver been matched to the actual impedance of each antenna:

> The proper impedance depends on the placement and excitation of the other elements. In fact, the optimum receiver input impedance is precisely the same as the optimum generator impedance for the same array for transmitting energy in the same direction.

This fact follows directly from the principle of reciprocity. It can be inferred directly, although it is by no means a simple exercise.

It should now be evident that mutual coupling plays an important role in the performance of array antennas. It may not be so evident that understanding and coping with its effects can be reduced to a reasonable problem. The remainder of this section is devoted to a detailed analysis of the ways in which mutual coupling depends on the design parameters of the array and its elements.

B. Effects of Mutual Coupling on Array Performance

The exact extent and nature of the effects of coupling on array performance depend on (1) the type of antenna and its design parameters, (2) the relative placement of the elements in the array, (3) the type of feed used to excite the elements and the design parameters thereof, and (4) the range of relative excitations employed (the scan volume of the array). In the following subsections, we will examine quantitatively the extent of these effects and their dependence on the factors mentioned. Before doing so, however, let us point out the practical consequences of these effects. These fall into two classes: (1) those effects which arise from the apparent variation in element driving impedance and (2) those which arise from the multipath nature of the route followed by the energy from each generator to the far field or from the incident wave to each receiver. These cause distortion of the array far-field pattern.

1. Impedance Variation and Its Subsidiary Effects on Equipment

The apparent variation in element impedance generally leads to a variation in array efficiency, since it is a practical impossibility to match the element driving impedance for all conditions of excitation. In addition, the apparent mismatch produces precisely the same effects as a real mismatch on such auxiliary equipment as receivers, transmitters, and transmission lines. Specifically, it can contribute to increasing the noise figure of the receivers and distort the receiver transfer coefficient in both phase and amplitude (leading in severe cases to receiver instability). On transmission, the transmitter transfer characteristic can be similarly altered. Also, on transmission, there are the possibilities of voltage breakdown and overheating in the transmitter output lines due to standing waves, and degraded transmitter output due to detuning.

2. Pattern Variation Effects

The multipath route the energy follows because of mutual coupling causes the patterns of arrays to differ from those that would be predicted on the basis of simple theory using noninteracting elements. In very large regular arrays (those in which the elements are placed at regular intervals on a grid and which have a sufficient number of elements so that edge effects can be ignored), the usual pattern distortion effect is a simple scaling up and down of the relative amplitude of the patterns while preserving the relative pattern shape. However, for irregular arrays or for small regular arrays with dominating edge effects, the relative pattern differs substantially, in ways which are often quite complicated, from the pattern computed ignoring coupling effects.

In antennas with elements that can support more than one orthogonal sense of polarization, it is possible for the coupling to excite the polarization sense which is not directly excited by the generators, thus causing depolarization of the signal.

Both the change in polarization and the change in efficiency due to mismatch effects cause the gain of the array to change as a function of the relative excitation of the elements; for example, the gain varies with scan angle (element-to-element phasing) in phase-scanned arrays.

II. COUPLING IN INFINITE REGULAR ARRAYS

As an aid to analysis and understanding, it is helpful to analyze an idealized array which, although a strict physical impossibility, is close enough to the real world to provide directly useful answers in many cases of practical importance, and insight into others.

A. Infinite Array Concept and Its Utility

The most useful idealized array model for coupling studies is usually referred to simply as an "infinite array." This means an array with (1) all elements placed at regular intervals either in a straight line or on a flat surface of infinite extent, (2) all elements identical, (3) the amplitude of element excitation equal from one element to another (uniform amplitude illumination), and (4) the relative phasings of the elements differing at most by a term which is linear in two orthogonal directions across the array. Mathematically, if the array lies in the x-y plane of a coordinate system such as that of Fig. 3 (centering one element for convenience), the elements

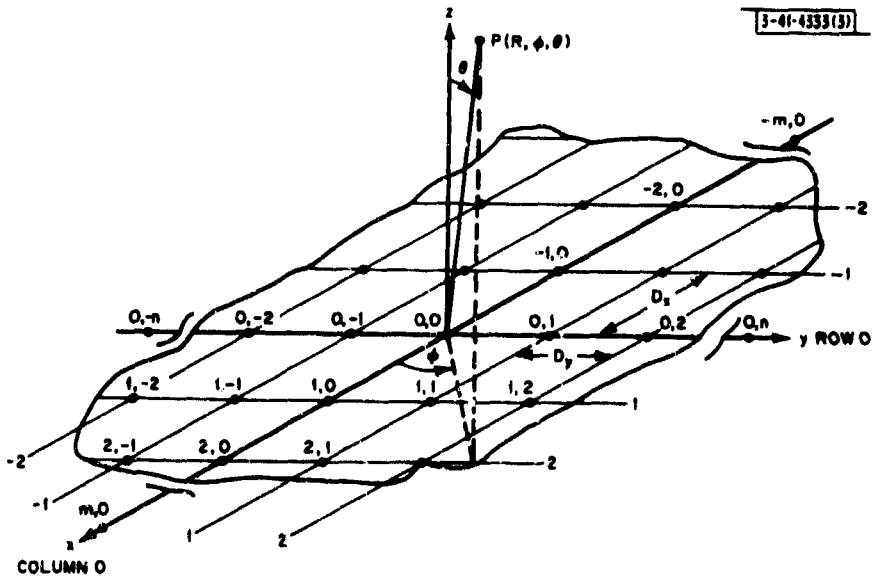

Fig. 3. Generalized planar array geometry.

are located at the intersections of a rectangular grid† with spacings D_x and D_y. Thus, it is convenient to represent elements by a double set of indices, so that the mn^{th} element is located at $x = mD_x$, $y = nD_y$. The element excitations differ only by a phase term

$$\phi_{mn} = m\alpha + n\beta$$

where α and β are the row and column phase increments.

The utility of this model is in the simplifications that it permits in mathematically modeling and analyzing the coupling in an array. As will be seen, the behavior of such an infinite array describes fairly accurately the behavior of most of the elements of modest to large arrays that are either on flat surfaces or shallowly curved surfaces with a smoothly varying amplitude and phase taper.

The nature of the behavior of the element driving impedance as a function of scan angle is easily assessed in an infinite array. For an antenna which is fed by a single-mode transmission line, we can write the terminal voltage of any one antenna in terms of the current flowing in the others by simultaneous equations of the form

$$V_{mn} = \sum Z_{mn,\,pq} I_{pq} \tag{1}$$

where the equation defines $Z_{mn,\,pq}$ as the ratio of the terminal voltage at antenna mn due to a unity current flowing in antenna pq when all other antenna currents are zero. Hence, the $Z_{mn,\,pq}$ are termed "mutual impedances" when the indices mn and pq are different. The driving impedance of the mn^{th} antenna is, by definition,

$$Z_{D_{nm}} = \frac{V_{nm}}{I_{nm}} \tag{2}$$

$$= \sum_m \sum_n Z_{nm,\,pq} \frac{I_{pq}}{I_{nm}} \tag{3}$$

But the regularity of the array and its excitation requires that

$$I_{pq} = I_{oo}\, e^{j(p\alpha + q\beta)} \tag{4}$$

If we consider the central element for notational simplicity, we have

$$Z_D(\alpha, \beta) = \sum_m \sum_n Z_{oo,\,pq}\, e^{j(p\alpha + q\beta)} \tag{5}$$

which makes apparent the fact that the driving impedance for such an array is simply the vector sum of $Z_{oo,\,oo}$ and the so-called "phased mutual impedances" resulting from the excitation of the other antennas. The term $Z_{oo,\,oo}$ is the impedance looking into the central element with all others open-circuited so that the current at their feed points is zero. If so terminating the antennas causes the current to be zero everywhere on the element (as would be true for thin, gap-fed dipoles and slots, if the reference point is effectively at the gap), then setting $I_{pq} = 0$ is physically equivalent to removing the pq element, and $Z_{oo,\,oo}$ is numerically the impedance of a single isolated element. In most practical cases, it is very nearly the same. We will investigate the behavior of the mutual impedances further in Sec. III.

† The practical and important case of a triangular grid can be analyzed by vacating every other site of a rectangular grid.

Since Eq. (5) was obtained without reference to the feed system supplying the element excitations, we can state categorically that in any infinite planar array of single-mode elements, the driving impedance is given by a two-dimensional Fourier series in the phasing constants. The coefficients of the series are the complex mutual impedances between elements. The ramifications of this result will be explored more fully below.

A second virtue of the infinite array model is that its periodic nature allows us to attack boundary value problems by use of Fourier series (see for example the discussion of the grating-lobe series in Sec. II-D).

Finally, since the impedance behavior of an antenna in an infinite array of single-mode elements does not depend on the details of the circuit feeding the array, we can, by this artifice, separate the discussion of the intrinsic properties of antenna elements from the more complex problems of the interaction between the elements and the feeds. For a finite or irregular array, we cannot in general discuss antenna impedance as an isolated factor.

B. Other Useful Idealizations

Several other idealizations which are commonly used are: (1) The concept of a "single-mode antenna element": an element whose boundary conditions are such that any current that flows has to conform to a single unique spatial distribution. The infinitesimally thin half-wavelength dipole and the thin resonant slot are classical examples of this type of element. (An open waveguide which has substantial excitation of higher order modes at the mouth is not of this type.) (2) The concept of an "invisible feed." This idealized feed does not perturb the current distribution on the antenna and has no coupling to the other antennas nor to other feeds, nor does it cause any rescattering. (3) If the elements are above a ground plane, the ground plane is assumed to be infinite in extent and to have infinite conductivity.

C. Resistive Sheet Problem

The fundamental nature of the mutual coupling problem (or, more precisely, one of its ramifications – the change in impedance of an array with scan angle) is illustrated by examining the behavior of the reflection coefficient of a thin resistive sheet of infinite extent backed by an open circuit[7] so that there are no fields transmitted through the sheet [see Fig. 4(a)].†

The boundary condition imposed by such a sheet is that for $z = 0$, for all x and y, the ratio of the total tangential electric field to the total tangential magnetic field be numerically equal to the surface impedance of the sheet. We choose the surface resistivity of the sheet to be that of free space: $\xi = 120\pi$ ohms, so that the sheet is an exact match for a normally incident wave.

If we now move the source through an angle Θ_E from the normal in the y-z plane of Fig. 4(b), we can express the spatial dependence of the incident and reflected plane waves as

$$\vec{E}^i = \vec{E}_o^i \exp[-jk(y \sin\Theta_E + z \cos\Theta_E)]$$

where $\vec{E}_o^i$ has a tangential component

$$\vec{E}_{o\,tang}^i = E_o^i \cos\Theta_E$$

† As pointed out in Ref. 7, the open circuit is not realizable, nevertheless the model is useful as we shall see.

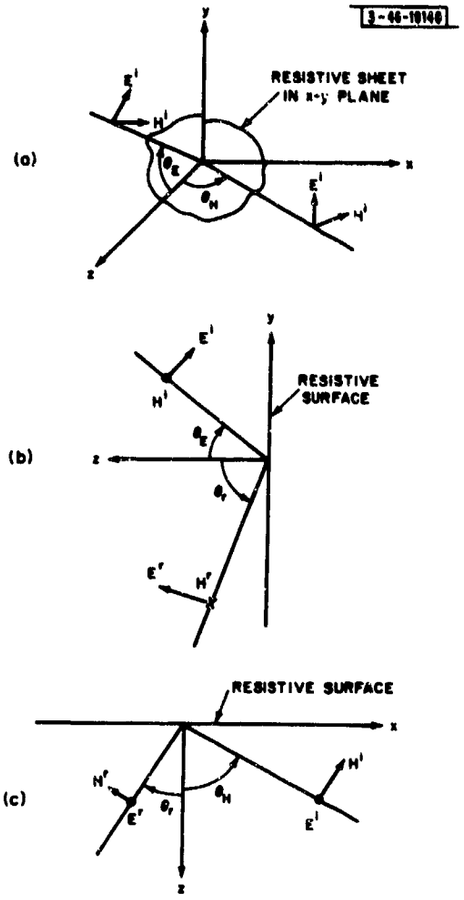

Fig. 4. Resistive sheet reflection geometry: (a) incident wave situations, (b) E-plane scan reflection, (c) H-plane scan reflection.

and

$$\vec{H}^{i} = \vec{H}_o^{i} \exp[-jk(y \sin\Theta_E + z \cos\Theta_E)]$$

where

$$\vec{H}^{i}_{o\,tang} = H_o^{i} \quad .$$

For the reflected wave, we have

$$\vec{E}^{r} = \vec{E}_o^{r} \exp[-jk(y \sin\Theta_r - z \cos\Theta_r)]$$

$$\vec{H}^{r} = \vec{H}_o^{r} \exp[-jk(y \sin\Theta_r - z \cos\Theta_r)]$$

with

$$\vec{E}^{r}_{o\,tang} = E_o^{r} \cos\Theta_r \quad , \quad \vec{H}^{r}_{o\,tang} = -H_o^{r} \quad .$$

Applying the boundary condition at z = 0 gives

$$\frac{E_o^i \cos\Theta_E \exp[-jky \sin\Theta_E] + E_o^r \cos\Theta_r \exp[-jky \sin\Theta_r]}{H_o^i \exp[-jky \sin\Theta_E] - H_o^r \exp[-jky \sin\Theta_r]} = \xi \quad .$$

For each wave, we also have

$$H_o^i = \frac{E_o^i}{\xi} \quad \text{and} \quad H_o^r = \frac{E_o^r}{\xi}$$

giving

$$E_o^i (\cos\Theta_E - 1) \exp[-jky \sin\Theta_E] + E_o^r (\cos\Theta_r + 1) \exp[-jky \sin\Theta_r] = 0 \quad .$$

This equation can obviously have a solution independent of y only if $\Theta_E = \Theta_r$. Making this substitution and solving for the voltage reflection coefficient gives

$$\Gamma_E = \frac{E_o^r}{E_o^i} = \frac{1 - \cos\Theta_E}{1 + \cos\Theta_E} \tag{6}$$

or

$$\Gamma_E = \tan^2 \frac{\Theta_E}{2} \quad . \tag{7}$$

By analogy to the transmission-line formula for the normalized load impedance r in terms of the reflection coefficient

$$\Gamma = \frac{r - 1}{r + 1}$$

the sheet represents an impedance to the wave that varies as

$$r_E = \frac{1}{\cos\Theta_E} \quad . \tag{8}$$

For scan in the H-plane, the assumed direction of E-field of Fig. 4(c) leads to

$$\Gamma_H = \frac{\cos\Theta_H - 1}{\cos\Theta_H + 1} \tag{9}$$

$$= -\tan^2 \frac{\Theta_H}{2} \tag{10}$$

and

$$r_H = \cos\Theta_H \quad . \tag{11}$$

Thus, even for such a simple situation as a wave impinging on a resistive sheet, there is a change in the apparent impedance that the sheet presents to the wave as a function of scan angle.

The practical importance of this result becomes apparent if we assume that the resistive sheet represents the limiting case of an array of infinitesimal dipoles with infinitesimal inter-element spacings. It is logical to expect on this basis that the reflection coefficient behavior represented by the sheet would be an extreme case. It might also seem logical that extremely dense packing of elements would represent maximum impedance variation; however, comparison

indicates the opposite is true. The resistive sheet impedance variation appears to represent a lower bound on impedance variation with scan.

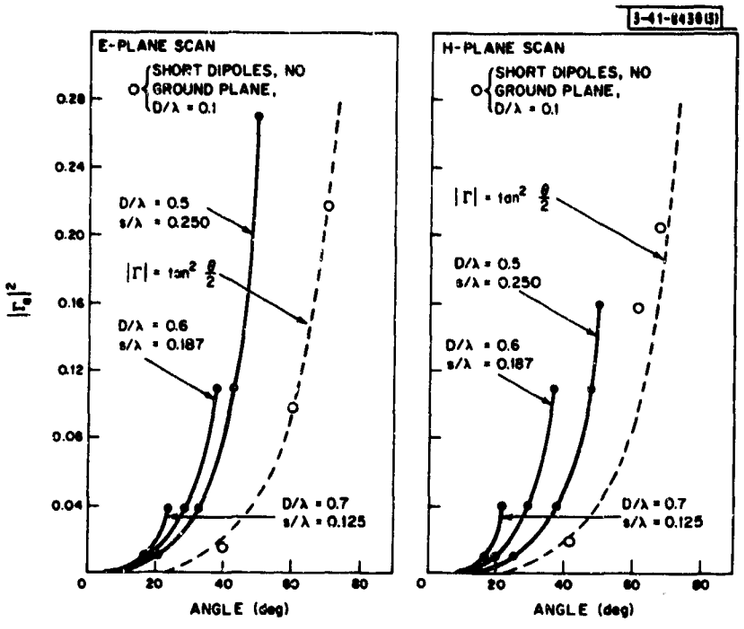

Fig. 5. Reflection coefficient magnitude vs principal plane scan angle.

For example, Fig. 5 compares the computed variation in reflection coefficient magnitude for arrays of half-wavelength dipoles for various spacings D and various heights s above a ground plane with the reflection coefficient behavior of the resistive sheet.† (The curves for wider spacings are discontinued at the angles where major lobes of the array are equally disposed about broadside; the behavior just retraces the curve from that point.) Note that the reflection coefficient for a given scan angle in the principal plane becomes monotonically better as the elements are brought closer together. As a confirmation, computations of the impedance behavior for a central element of a large array of short dipoles without a ground plane for $D_x = D_y = 0.1\lambda$ are also shown. It is apparent that the approximation to the impedance variation of the resistive sheet is quite good.

The second important consideration is the base from which this change takes place; in the figure, this is the impedance which matches the array at broadside. What the figure does not show is that for the very closely spaced short dipoles, the absolute impedance – particularly the reactive part – has become exceedingly large, although the change in impedance is quite small. All the data presented assume the generator impedance is matched to the element driving impedance when the array is phased for broadside reception or transmission. To do so, it is necessary to tune out the broadside driving reactance. If this reactance is large compared to the resistive part, the tuning is extremely critical; such is the case for short dipoles stacked close together.

† The height s in Fig. 5 is the one that minimizes the mismatch in the principal planes of scan.

D. Grating-Lobe Series and Its Significance

The periodic nature of the infinite array permits a very general analysis of the impedance-vs-scan behavior of various elements. By expressing the power radiated and the power stored in the vicinity of the array in terms of the current or field distribution on a typical element, the complete impedance behavior as a function of inter-element phasing can be described. The result, although in the form of an infinite series, is not only a useful computational tool for elements with known current distributions, but also furnishes insight into the properties of elements that affect their impedance behavior.

Pioneering in the analysis of infinite arrays was done by Wheeler[8] and Edelberg and Oliner,[9] but Stark[10] gave the first definite exposition of the complete series. Both Wheeler[11] and Parad[12] have written on the physical interpretation of the result, and Rhodes[13] has given an elegant derivation of a related expression for single elements. The derivation is straightforward, but will only be sketched here. It is based on the fact that from an expression for the total power flow (both real and reactive) outward from a typical cell of an infinite array at the array face, the driving impedance the cell presents to a single-mode transmission line can be calculated and shown to be related to the element pattern.

To illustrate, let us consider an array of elements on a rectangular grid. The elements are assumed to be identical metallic conductors of infinite conductivity with a known surface current density distribution in the y-direction, $K_y(x, y)$.† The surface current density is identical from cell to cell, except that the relative phase of the current at the center of the mn^{th} cell is $\exp[-j(m\alpha + n\beta)]$. Thus, the total surface current density distribution can be expressed as a doubly infinite series:

$$\overline{K}(x, y) = \bar{e}_y \sum_m \sum_n K_y(x - mD_x, y - nD_y) \exp[-j(m\alpha + n\beta)] \tag{12}$$

where $\bar{e}_y$ is the y-directed unit vector. Note that $\overline{K}(x, y)$ is not a periodic function; however, the product $\overline{K}(x, y) \exp[j(\alpha x/D_x + \beta y/D_y)]$ is periodic and can be expanded in a two-dimensional Fourier series. The result is that the normalized current density can be written as

$$\frac{\overline{K}(x, y)}{I_{inc}} = \bar{e}_y \sum_p \sum_q K_{y_{pq}}(\alpha, \beta) \exp[-j(k_{x_p} x + k_{y_q} y)]$$

where we have defined

$$k_{x_p} = \frac{\alpha + 2p\pi}{D_x} \tag{13a}$$

$$k_{y_p} = \frac{\beta + 2q\pi}{D_y} \tag{13b}$$

and

$$k_{z_{pq}} = \sqrt{k_o^2 - k_{x_p}^2 - k_{y_q}^2} \quad . \tag{13c}$$

† Only the requirement of identical elements is necessary; the other restrictions are for convenience and can be removed.

The definition of $k_{z_{pq}}$ is included for later reference, and k_o is the free-space propagation constant, $k_o^2 = \omega^2 \mu_o \epsilon_o$. By the usual procedure, the Fourier coefficients are found to be

$$K_{y_{pq}}(\alpha, \beta) = \frac{1}{D_x D_y} \int_{-D_x/2}^{D_x/2} \int_{-D_y/2}^{D_y/2} \frac{K_y(x, y)}{I_{inc}} \exp[j(k_{x_p} x + k_{y_q} y)] \, dxdy \quad . \tag{14}$$

If we now apply Maxwell's equations to the free-space region in front of the array, we obtain expressions for the electric and magnetic fields in space in terms of the surface current density at the aperture. The electromagnetic fields in space must be periodic in the same sense as the surface current density and, in fact, must be an infinite set of propagating or attenuating plane waves. For the electric and magnetic fields tangential to the aperture plane, we have

$$H_x(x, y, z) = \sum_p \sum_q \frac{K_{y_{pq}}(\alpha, \beta)}{2} \exp[-j(k_{x_p} x + k_{y_q} y + k_{z_{pq}} z)] \tag{15a}$$

$$E_y(x, y, z) = \frac{-\xi}{2k_o} \sum_p \sum_q \frac{(k_o^2 - k_{y_q}^2) K_{y_{pq}}(\alpha, \beta)}{k_{z_{pq}}} \exp[-j(k_{x_p} x + k_{y_p} y + k_{z_{pq}} z)] \tag{15b}$$

where $\xi = \sqrt{\mu_o / \epsilon_o}$ is the intrinsic impedance of free space.

It should be noted that the wave equation for the free-space region defines an infinite spectrum of plane waves. Each plane wave is associated with a "propagation vector" with components k_x, k_y, and k_z. In general, these components can be complex, but for this case, k_x and k_y are constrained to be real, while k_z is positive real or negative imaginary such that the wave equation will be satisfied:

$$k_z^2 = k_o^2 - k_x^2 - k_y^2 \quad , \quad k_o^2 = \omega^2 \mu_o \epsilon_o \quad .$$

Physically, for $k_x^2 + k_y^2 \leq k_o^2$, we can identify the k's with the angles of Fig. 3:

$$\begin{aligned} k_x &= k_o \sin\Theta \cos\phi \\ k_y &= k_o \sin\Theta \sin\phi \\ k_z &= k_o \cos\Theta \quad . \end{aligned} \tag{16}$$

In this notation, for example, the far field of a typical element with normalized current density $[K_y(x, y)/I_{inc}] \, e_y$ is

$$\sqrt{1 - \left(\frac{k_y}{k_o}\right)^2} \int_{-D_x/2}^{D_x/2} \int_{-D_y/2}^{D_y/2} \frac{K_y(x, y)}{I_{inc}} \exp[j(k_x x + k_y y)] \, dxdy$$

where I_{inc} is the total incident current in a cell. The usual pattern in ϕ and Θ coordinates is obtained by substitution of Eqs. (16) into this result. Note that the Fourier components of the current density are related to the far-field pattern of an element when $k_{x_p}^2 + k_{y_q}^2 \leq k_o^2$. Although we cannot associate the plane waves that have $k_x^2 + k_y^2 > k_o^2$ with the element radiation pattern, they still have significance because they correspond to stored energy in the aperture.

It is also worth noting that the discrete, periodic boundary condition defined by the aperture of the array causes the radiated power to be confined to a discrete set of directions in $k_x k_y$-space.

In the above notation, this means that the variables k_x and k_y take on only the discrete set of values k_{x_p} and k_{y_q} for every beam-pointing angle specified by the element phasings, α and β. This contrasts with the situation for finite, planar apertures where k_x and k_y are continuous variables.

If the normal component of the Poynting vector, $-E_y H_x^*$, is integrated over one cell in the aperture plane, we obtain an expression for the complex radiated power per element. The element driving impedance is related to the radiated power and is given by

$$Z_D(\alpha,\beta) = \xi \frac{D_x D_y}{2k_o} \sum_{p=-\infty}^{\infty} \sum_{q=-\infty}^{\infty} \frac{(k_o^2 - k_{y_q}^2)}{k_{z_{pq}}} |K_{y_{pq}}(\alpha,\beta)|^2 \quad . \tag{17}$$

Observe that the numerator in the p = q = 0 term is just the power pattern of an element of the array when $(\alpha/D_x)^2 + (\beta/D_y)^2 \leq k_o^2$.

1. Physical Interpretation of the Series

To grasp the significance of the "directions" specified by the factors k_{x_p}, k_{y_q}, and $k_{z_{pq}}$, note that we can write the array factor of a uniformly illuminated array with phase constants α and β as

$$A(k_x, k_y) = \sum_m \sum_n \exp[j(m\alpha + n\beta)] \exp[-j(k_x m D_x + k_y n D_y)] \quad .$$

As it stands, A is a function of two variables k_x and k_y that can range from $-\infty$ to $+\infty$. It will have maxima at points "in k-space" where

$$(k_x D_x - \alpha) = p2\pi$$

$$(k_y D_y - \beta) = q2\pi$$

or, referring to Eq. (17), at all values of k_x and k_y satisfying

$$k_x = k_{x_p} \quad , \quad p = 0, \pm 1, \pm 2, \ldots$$

$$k_y = k_{y_p} \quad , \quad q = 0, \pm 1, \pm 2, \ldots \quad .$$

That is, the infinite array generates a "nest" of delta functions in k-space on a regular grid as indicated in one dimension in Fig. 6(a). The delta functions inside

$$k_x^2 + k_y^2 = k_o^2$$

correspond to grating lobes in visible space, the remainder to lobes in "invisible space."

Consequently, we have a physical interpretation of each term of Eq. (17): the pq term corresponds in amplitude to the element "power pattern" [Fig. 6(b)] of a typical element in the "direction" k_{x_p}, k_{y_q} divided by the z-direction "propagation" constant [Fig. 6(c)]. For k_{x_p} and k_{y_q} in real space, the z-direction propagation constant is real and that term of the series contributes only to the real part of the impedance. If k_{x_p} and k_{y_q} are large enough to make $k_{z_{pq}}$ imaginary, that entire term will be imaginary and will contribute only to the reactance.

An important observation about the symmetry of the driving impedance variation with scan follows from the fact that substitution of $-\alpha$ and $-\beta$ into Eqs. (13) for k_{x_p} and k_{y_q} changes

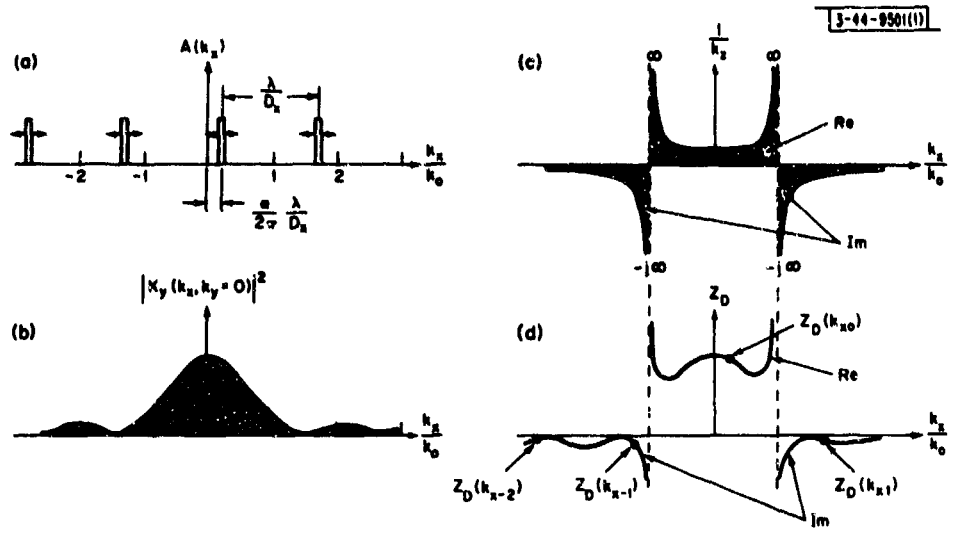

Fig. 6. Factors of grating-lobe series (one dimensional): (a) scanning array of delta functions, (b) element pattern, (c) $1/k_z$ factor, (d) resulting contributions to series for $Z_D(\theta)$.

$k_{x_p} \rightarrow -k_{x_{(-p)}}$, etc. Since we sum over all p and q, the signs of p and q are unimportant. Further, since $K_{y_{pq}}(\alpha, \beta)$ is multiplied by its complex conjugate in Eq. (17), the sign $Z_D(\alpha, \beta)$ is invariant to changes in sign of k_{x_p} and k_{y_q}; hence,

$$Z_D(\alpha, \beta) = Z_D(-\alpha, \beta) = Z_D(\alpha, -\beta) = Z_D(-\alpha, -\beta) \tag{18}$$

for an element in an infinite array. Thus, in the following examples, we will only examine the behavior of $Z_D(\alpha, \beta)$ for positive α and β.

2. Some Qualitative Inferences from the Series

The effect of scanning the beam on the driving impedance of the element thus depends on the change of the sum of the contributions of the individual grating lobes as the nest of grating lobes is scanned in k-space. For example, the effect of a grating lobe crossing the boundary between real and imaginary space depends markedly on the behavior of the element pattern at that boundary, since $1/k_z = \infty$. Unless the element pattern has a null in that direction, a discontinuity in impedance occurs as the grating lobe crosses over this boundary, and abruptly changes its contribution from reactance to resistance or vice versa.

The limiting cases of the effect of element spacing on the element impedance variation can be easily assessed from the grating-lobe series. In the limiting case, as the spacing approaches zero, the grating lobes recede toward infinity. As the elements shrink to accommodate the spacing, the current density becomes a constant for all cells, and the element power pattern, the numerator in the summation of Eq. (17), is just the "obliquity factor," $1 - k_y^2/k_o^2$. The pq term of the series thus has the following asymptotic behavior for large k_{x_p} and k_{y_q} (small D_x and D_y)

$$\frac{k_o^2 - k_{y_q}^2}{k_o k_{z_{pq}}} \longrightarrow \begin{cases} -jk_{y_q} & \text{along the } k_y \text{ axis} \\ \dfrac{-j}{k_{x_p}} & \text{along the } k_x \text{ axis} \end{cases}$$

and consequently the reactance becomes very large due to the impulses at large values of k_y. However, the variation in impedance due to the lobes other than p = q = 0 tends to zero, since the amount of phase differential β/D_y between elements required to steer a beam to a given angle is constant and, therefore,

$$\lim_{D_x \to 0} k_{y_q} = \frac{2\pi}{D_y}$$

which is independent of element phasing. Only the impedance contribution of the p = q = 0 term varies, and the fractional variation in R_D is seen from Eq. (17) to be

$$r = \frac{R_D(\alpha, \beta)}{R_D(0, 0)} = \frac{1 - \sin^2\Theta \sin^2\phi}{\cos\Theta} \quad .$$

For E-plane scan, $\phi = \pi/2$ and

$$r_E = \cos\Theta$$

while for H-plane scan, $\phi = 0$ and

$$r_H = \frac{1}{\cos\Theta}$$

in agreement with Eqs. (8) and (11) for the resistive sheet and the trend indicated by the examples of Fig. 5, if account is taken of the fact that Eqs. (8) and (11) are for the impedance looking into the array from space. The above results are for the impedance looking out. The normalized impedance is thus inverted.

For widely separated elements of small active area, the grating-lobe series indicates exactly what intuition suggests: as the element separation increases, the impulses move very close together so that many are in visible space, and scanning the array merely moves some out of visible space and others into it, with a net result of little impedance variation with scan. Of course, as a consequence, there are also numerous lobes in the actual spatial pattern in visible space, as indicated in Fig. 7, with resulting loss of sensitivity and potential directional ambiguity.

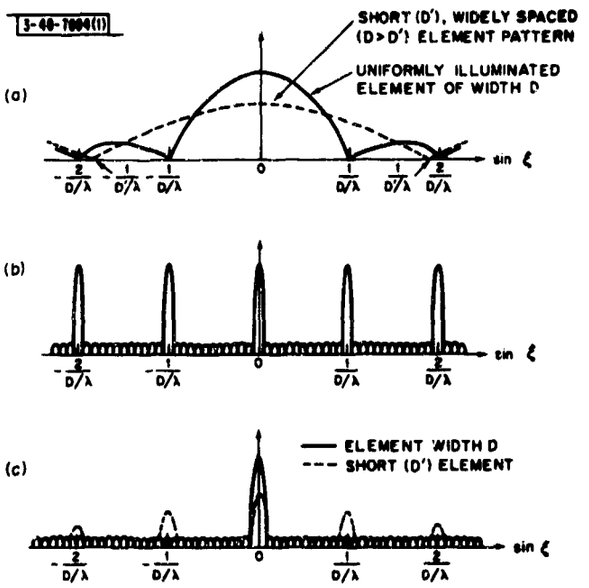

Fig. 7. Effect of element size on array patterns: (a) element pattern, (b) array factor for element spacing D, (c) far-field pattern.

Of more practical interest for elements with widely separated centers is the case in which the elements are themselves directive. One way to achieve this is to have the current distribution occupy most of the space between the elements, such as using parabolic reflectors. The pattern result is indicated in Fig. 7: using more of the allotted space improves the suppression of the grating lobes. In the limit, as we fill all allotted space with a uniform current distribution, the pattern grating lobes are completely suppressed when the beam is pointed at broadside. However, they are only partially suppressed as the beam is scanned. The same thing is taking place in the grating-lobe series; the wide center-to-center element spacing places many of the nest of impulses in visible space, but these are suppressed to a degree which depends on the extent to which the aperture is filled.

3. Additions to the Basic Series

Several interesting and useful additions can be made in the basic grating-lobe-series formulation. First, as Stark has pointed out, the modification of Eq. (17) that must be made to accommodate elements above an infinite, perfectly conducting ground plane consists of the addition of a factor dependent on the element-to-ground-plane spacings:

$$Z_D(\alpha,\beta) = \xi \frac{D_x D_y}{2k_o} \sum_{p=-\infty}^{\infty} \sum_{q=-\infty}^{\infty} \frac{(k_o^2 - k_{y_q}^2)}{k_{z_{pq}}} |K_{y_{pq}}(\alpha,\beta)|^2 \{1 - \exp[-j2k_{z_{pq}} s]\} \quad . \tag{19}$$

This additional factor is of no small importance, since it goes to zero whenever $k_{z_{pq}} = 0$ in the denominator. The effect on impedance variation is pronounced, as we shall see.

The grating-lobe series is also adaptable to any regular grid of elements (e.g., triangular). It is only necessary to set the relative spacings and placement of the nest of impulses to correspond to the grid shape and spacing.

The series can also be used to infer the approximate average (with respect to position in the array) impedance behavior of the elements of small arrays of identical elements. The infinite array assumption in the derivation is responsible for two aspects of the results of Eqs. (17) and (19):

(a) Justification for assuming that all elements have the same impedance and known relative amplitude and phase weighting (see Sec. II-A). Therefore, the impedance of any particular element is simply related to the variation in radiated and stored power of the entire array.

(b) The sampling functions (the nest of delta functions of Fig. 6) have infinitesimal width.

Thus, to apply the grating-lobe series to small arrays, we must be willing to settle for an approximate average behavior of the elements (approximate, since we still assume in the derivation that the relative amplitudes and phases of the elements are known, which actually depend on the relative impedances). If we accept this shortcoming, the effect of the small array is to replace the delta functions with sampling functions of a width equal to the array beamwidth. The net effect is that a reasonable qualitative assessment of the small array impedance variation can be obtained from that of the infinite array by averaging the infinite array data over a beamwidth of the small array.

Finally, the series can be extended to include arrays of crossed-dipole pairs with or without ground planes. Since the orthogonal dipoles are radiatively coupled to each other at nearly

all scan angles, the analysis of this type of array is more complicated. That is, the radiative coupling will influence the relative currents on the dipoles of every pair with the result that the type of feed network behind every dipole pair must be included in the analysis. The problem can still be formulated in rather general terms for arbitrary three- or four-port feed networks behind every dipole pair; however, we must completely specify the parameters (scattering matrix, for example) of the feed network before valid numerical results can be obtained. In the analysis of this type of array, we must consider the polarization properties of the transmitted waves, the impedance variation at the input port (or ports) of the feed network for a dipole pair, and the power dissipated in the feed network or its termination.

E. Dependence of Element Impedance on Element and Array Design Parameters

In this section, we present results of the dependence of the element driving impedance $Z_D(\alpha, \beta)$ on the pointing direction of the main beam of the array. We first examine in a planar array context the extent to which the impedance variation can be expected to depend on element type and spacing and other design details. We then examine the difference in behavior in linear arrays, including a brief examination of the frequency dependence of the driving impedance.

1. Planar Array Impedance Behavior

To make the data more directly useful for design, we will discuss Z_D for planar arrays as a function of the scan angles in each of three planes through array broadside. The symbols Θ_E, Θ_H, and Θ_D will be used to define the angle of the beam from broadside in the E-plane, H-plane, and "diagonal (D)" plane (45° from both E and H), respectively. If the elements are polarized in the y-direction, we can make the correspondence between α, β, and Θ_E, Θ_H, and Θ_D by

$$\alpha = \frac{-2\pi D_x}{\lambda} \sin\Theta_H \quad , \quad \text{H-plane scan}$$

$$\beta = \frac{-2\pi D_y}{\lambda} \sin\Theta_E \quad , \quad \text{E-plane scan}$$

$$\sqrt{\frac{\alpha^2}{D_x^2} + \frac{\beta^2}{D_y^2}} = \frac{2\pi}{\lambda} \sin\Theta_D \quad , \quad \text{D-plane scan} \quad .$$

The data presented were computed from Eqs. (17) and (19), as appropriate, using a digital computer to sum several hundred terms. To provide a crude assessment of the dependence of impedance variation on element type, three significantly different current distributions within a cell were examined:

(1) An idealized short dipole; infinitesimal diameter, effective length 0.1λ.

(2) An idealized half-wavelength dipole; infinitesimal diameter, $K_y(y) = K_o \cos \pi y/\lambda$.

(3) A uniform current sheet filling the entire D_x by D_y cell.

Models (1) and (2) represent idealized models of both dipoles and their complement, slots in an infinite ground plane. Model (3) is a crude but tractable model of the dual of an open-waveguide radiator. It has recently been demonstrated experimentally that model (2) accurately predicts the behavior of real dipole arrays[14] even for lengths not particularly close to a half wavelength. Some experimental data on open waveguide array behavior are presented later.

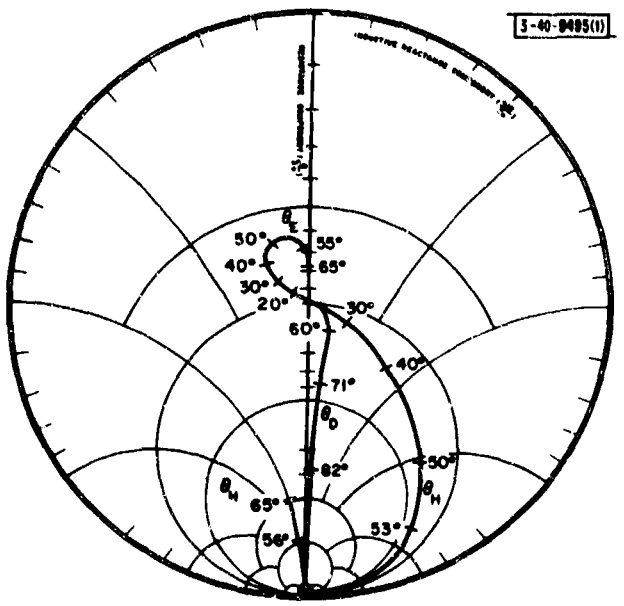

Fig. 8. Normalized impedance vs scan angle in E-, H-, and D-planes for a typical element of an array of short dipoles ($L = 0.1\lambda$); $D_x = D_y = 0.55\lambda$.

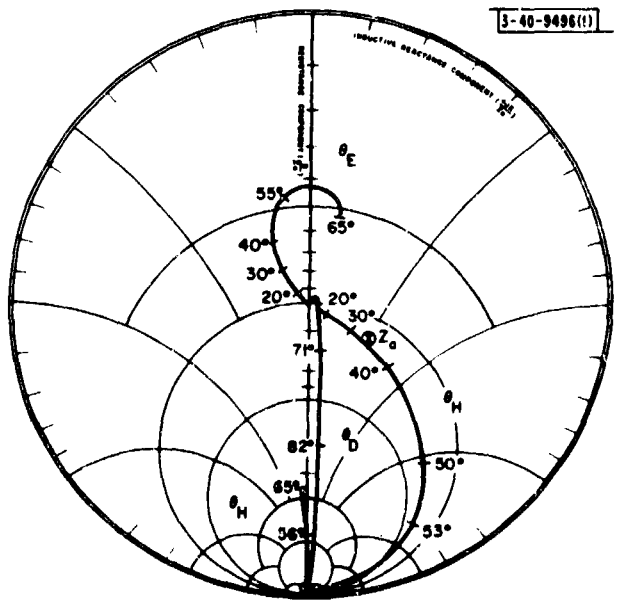

Fig. 9. Normalized impedance vs scan angle in E-, H-, and D-planes for a typical element of an array of $\lambda/2$ dipoles; $D_x = D_y = 0.55\lambda$.

We first compare the impedance behavior of these three models in a common configuration – a planar array with elements on a 0.55λ square grid (maximum scan without grating lobes: 55° in E- and H-planes). We then examine the modification of the dipole behavior when a ground plane is used. The effect of element spacing and grid shape on impedance variation is assessed for dipoles above ground, and the interplay between element spacing and ground plane height is examined as an indication of the extent to which the designer can optimize performance. The behavior of linear arrays is briefly examined and compared with planar array behavior. Finally, we present an example of the frequency dependence of the driving impedance.

For uniform presentation of the data in a useful form, Z_D vs angle is displayed on Smith charts (see Fig. 8). We present normalized Z_D, i.e., for $Z_D(\Theta) = R_D(\Theta) + jX_D(\Theta)$,

$$Z_D(\Theta)_{norm} = \frac{Z_D(\Theta) - jX_D(0)}{R_D(0)} \tag{20}$$

where 0 refers to the value of Z_D when the beam is pointed at broadside. While not the only choice of interest, there are three reasons for this format:

(a) It displays the impedance variation as it would occur if the array were matched at broadside – a condition that maximizes gain (but does not minimize impedance variation).

(b) It makes the results easier to correlate with experimental measurements; the effects of any actual matching networks in the antenna are accounted for by normalizing, except for an arbitrary rotation of the Smith chart.

(c) In some cases, the grating-lobe series does not converge to a unique Z_D, but does converge to a unique value of $[Z_D(\Theta) - jX_D(0)]/R_D(0)$.

To aid the reader, for model (2), which is used for comparison of different array configurations, we will include $Z_D(0)$ and also the impedance of a single isolated element (above a ground plane if appropriate), Z_a (see Fig. 9).†

2. Comparison of Element Types

Figure 8 shows the behavior of a typical element of an array of short dipoles (SD) [for short slots, interchange E for H and impedance for admittance]. The most striking fact is the superiority of the behavior in the E-plane over the other planes. Unfortunately, the E-plane is atypical, since the factor $(k_o^2 - k_{y_q}^2)$ has a zero in the E-plane at the same angle as the zero of k_z in the denominator of Eq. (17). For all other scans, the impedance goes to the edge of the Smith chart whenever

(a) A grating lobe comes into visible space, which occurs at 55° in the H-plane, or

(b) The main lobe is scanned out of visible space, which occurs at 90° in the D-plane.

The E- and H-plane curves are discontinued at 65°. This angle physically corresponds to a grating lobe at −65° (symmetrically disposed relative to the main beam), so that further scanning is equivalent to scanning the main beam in from 65°; the curve retraces itself.

If we adopt as an arbitrary criterion a tolerable VSWR of 3:1, we can scan to about 47° in the H-plane, about 79° in the D-plane, and anywhere in the E-plane; for a 2:1 VSWR, 40° in H, 76° in D, and anywhere in E.

† For wide scan angles, a match to Z_a very nearly minimizes the mismatch with scan, but at a loss in broadside gain with respect to a match to $Z_D(0)$.

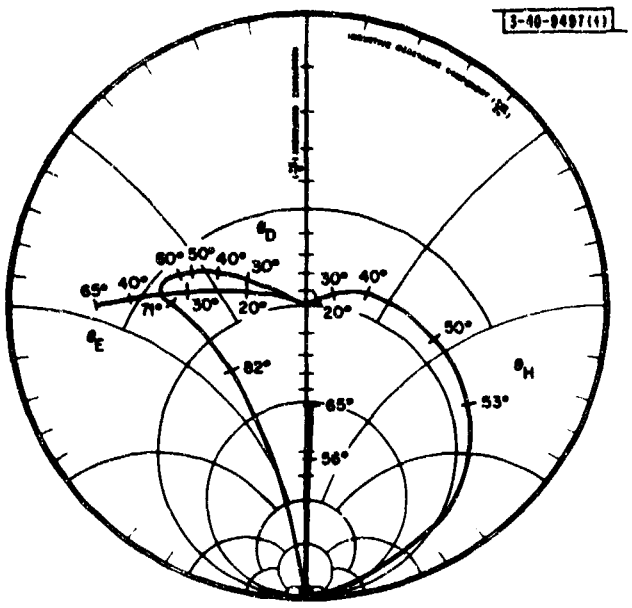

Fig. 10. Normalized impedance vs scan angle in E-, H-, and D-planes for a typical element of an array of uniformly illuminated cells; $D_x = D_y = 0.55\lambda$.

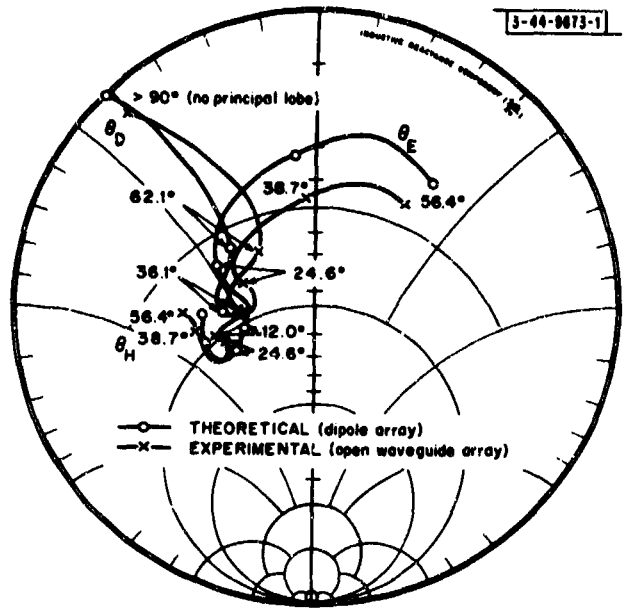

Fig. 11. Comparison of measured impedance variation of a central element in a 10 × 10 open-waveguide array with that computed for the same element in an identical array of $\lambda/2$ dipoles without ground plane; $D_x = D_y = 0.6\lambda$.

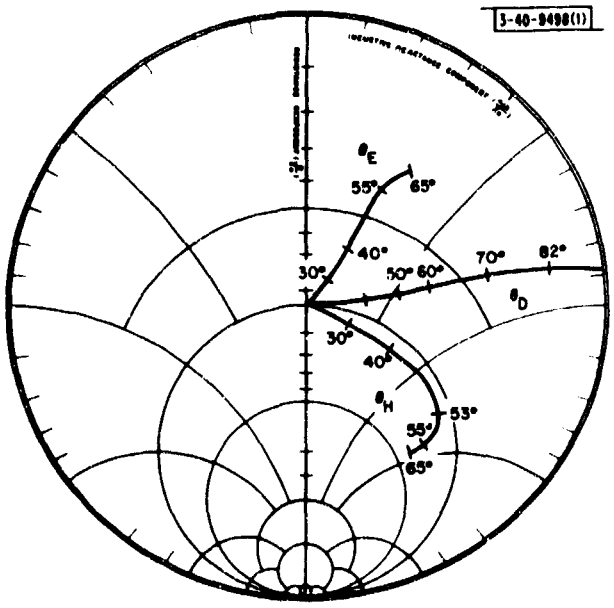

Fig. 12. Normalized impedance vs scan angle in E-, H-, and D-planes for a typical element of an array of short dipoles ($L = 0.1\lambda$) mounted 0.25λ above ground plane; $D_x = D_y = 0.55\lambda$.

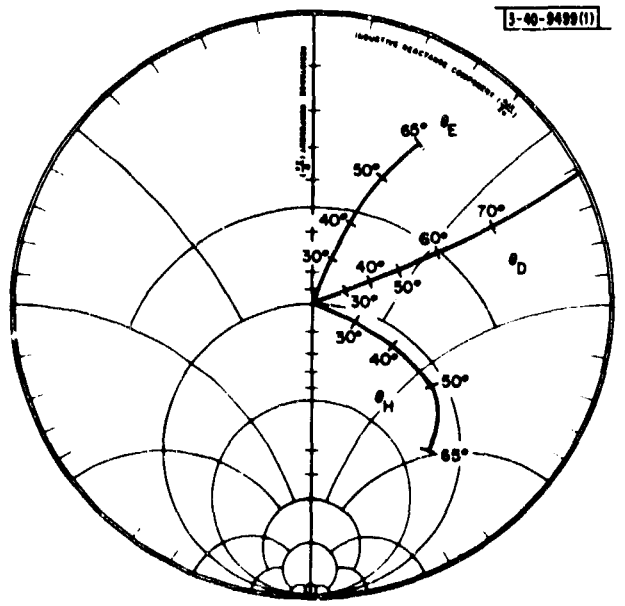

Fig. 13. Normalized impedance vs scan angle in E-, H-, and D-planes for a typical element of an array of $\lambda/2$ dipoles mounted 0.25λ above ground plane; $D_x = D_y = 0.55\lambda$.

For a half-wavelength dipole (HD), as indicated in Fig. 9, the behavior is qualitatively quite similar, suggesting that the dipole length is of secondary importance. For a 3:1 VSWR, we can scan to about 45° in H, 79° in D, and anywhere in E; for a 2:1 VSWR, about 40° in H, 77° in D, and 50° in E.

The "open-waveguide" (OWGD) dual model shows a still greater E-plane variation than either dipole, but is again qualitatively similar (an observation made more obvious by comparing the OWGD dual model results of Fig. 10 with Fig. 9 rotated about 45° ccw). For a 3:1 VSWR, we can scan about 51° in H, about 75° in D, and about 35° in E; for a 2:1 VSWR, about 42° in H, 45° in D, and about 28° in E.

These results are summarized in Table I.

TABLE I

IMPEDANCE BEHAVIOR OF ELEMENTS WITHOUT GROUND PLANES

VSWR	Scan Plane	Element Type		
		SD	HD	OWGD
3:1	E	–	–	35
	H	47	45	51
	D	79	79	75
2:1	E	–	50	28
	H	40	40	42
	D	76	77	45

Since the OWGD dual model is crude, its apparent inferiority should not be taken too seriously. To reinforce this point of view, Fig. 11 shows a comparison of experimentally determined Z_D for a finite (10 × 10) array of open-waveguide radiators with computations for a similar (10 × 10) array of half-wavelength dipoles without a ground plane. In this case, the impedance variation of the element in the waveguide array is seen to be slightly less than that for the same element in the dipole array for scan in the waveguide E-plane (the H-plane for dipoles). For scan in the waveguide H- and D-planes, however, the results for the two arrays are within the limits set by experimental tolerances. Similar results were obtained for other elements in this particular array and for waveguide and dipole arrays with different inter-element spacings ($D_x = 0.6\lambda$, $D_y = 0.3\lambda$). The obvious conclusion is that the impedance behavior of an element in a waveguide array can be predicted reasonably well by computations on a similar array of dipoles.

The addition of a ground plane under the dipoles has a marked effect on the impedance behavior as shown in Figs. 12 and 13 for the short and half-wavelength dipoles. Physically, the addition of the ground plane below an electric dipole prevents the dipole from radiating along the ground plane; hence, in the language of the grating-lobe series of Eq. (19), the ground plane factor, $1 - \exp[-j2k_z s]$, approaches zero as $k_z \to 0$, so that the impedance is continuous when a grating lobe becomes visible. Also, if an element can radiate in the direction of the other elements, a grating lobe directed toward the other elements will cause them to absorb as much power as they radiate, bringing about a unity reflection coefficient.

The diagonal plane scan still causes the reflection coefficient to reach a magnitude of unity, since the beam can be scanned out of visible space without a grating lobe coming into visible space, thus suppressing all radiation (for an infinite array).

For the elements mounted a quarter-wavelength above ground, the allowable scans for 3:1 and 2:1 VSWR's are as shown in Table II.

TABLE II

IMPEDANCE BEHAVIOR OF ELEMENTS WITH GROUND PLANES

VSWR	Scan Plane	Element Type SD	Element Type HD
3:1	E	55	50
	H	50	50
	D	62	62
2:1	E	45	40
	H	40	40
	D	52	50

The differences between the short- and half-wavelength dipole array results are not significant, particularly in view of the ability to alter the impedance behavior somewhat by varying s, as we shall see.

In summary, the most striking difference in impedance behavior of the elements investigated is brought about by suppressing the ability of an element to radiate in the direction of other elements. For dipoles and some similar elements, this can be easily accomplished by placing them above a ground plane. Note, however, that slots or open waveguides in a ground plane do radiate along the ground plane and hence are analogous in behavior to a dipole without a ground plane (the thin slot in a ground plane is the exact dual of the dipole without a ground plane).

Even this difference in behavior is only important for scan angles near grating-lobe formation. It is evident from Tables I and II that if the usual element spacing criterion of allowing a grating lobe to appear marginally is used to design the array, elements such as dipoles would give vastly superior (but still poor) VSWR performance at extreme scans if placed above a ground plane. If, however, the element spacing is chosen to constrain the maximum VSWR to a reasonable value, there appears to be little difference between the elements, and other considerations (e.g., mechanical convenience) should dictate the choice. Note, however, that such a criterion results in a much smaller allowable scan volume for a given element grid spacing.

To illustrate the extent to which detailed design parameters may affect impedance behavior, we will explore the interlocking effects of two parameters of an array of dipoles above ground. We will also examine the effect of the height of the dipole above ground, s, on the maximum VSWR which occurs for a specified scan volume. In particular, we will choose a 40° cone-shaped scan volume and examine elements on a square grid (suggested by the symmetry of the scan volume) and a triangular grid.

A plot of maximum VSWR as a function of ground plane spacing is shown in Fig. 14 for E- and H-plane scans of two square-grid arrays. From this figure, it is apparent that the maximum

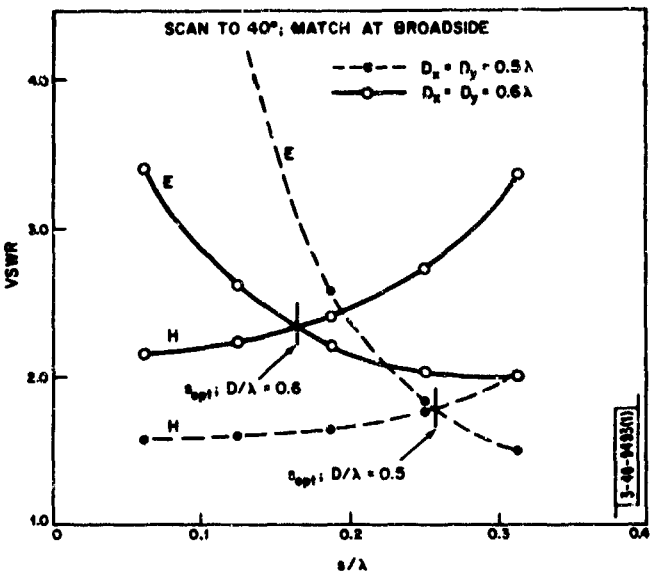

Fig. 14. VSWR at θ_{max} vs ground plane spacing for large, square-grid arrays of $\lambda/2$ dipoles.

E-plane mismatch becomes very large and the maximum H-plane mismatch becomes monotonically smaller as the ground plane spacing is decreased. Thus, for every inter-element spacing, there is an optimum ground plane spacing which equalizes the maximum mismatch in the principal planes of scan for a specified scan volume.

A similar set of computations for planar arrays with the elements on an equilateral triangular grid is shown in Fig. 15 for a scan of 40°. Qualitatively, the results are quite similar to those for the square-grid planar arrays. In particular, for every inter-element spacing, there is an optimum element-to-ground-plane spacing which minimizes the maximum mismatch (assuming a match at broadside) incurred for a conical scan volume.

Figure 16 shows a plot of impedance variation with scan angle for a triangular-grid array mounted at the optimum height above the ground plane (compare with Fig. 13 for the square-grid array).

A cursory examination of the data for square-grid and triangular-grid arrays with approximately equal areas per element indicates that the triangular-grid array may be preferable on the basis of impedance variation, although the difference is slight. Further, the comparison is not direct, since the two arrays have somewhat different spatial coverages.

For all the linear- and planar-array configurations, it is seen that for optimum ground plane spacing for a given volume coverage, an array with elements more closely spaced than required by grating-lobe considerations will exhibit <u>less</u> impedance variation than one which just satisfies the scan volume requirement: this is, of course, obtained at the expense of a larger number of elements to realize the same gain and beamwidth.

3. Linear Array Impedance Behavior

For a planar array with different scan requirements in the x- and y-directions, an additional design parameter is the choice of element alignment with the x- and y-axes. This is most evident in what we might view as an extremely degenerate case: a linear (one-dimensional) array. Furthermore, linear arrays are obviously of interest in their own right. Consequently, we will briefly examine the difference in impedance behavior, using arrays of dipoles above ground for illustration.

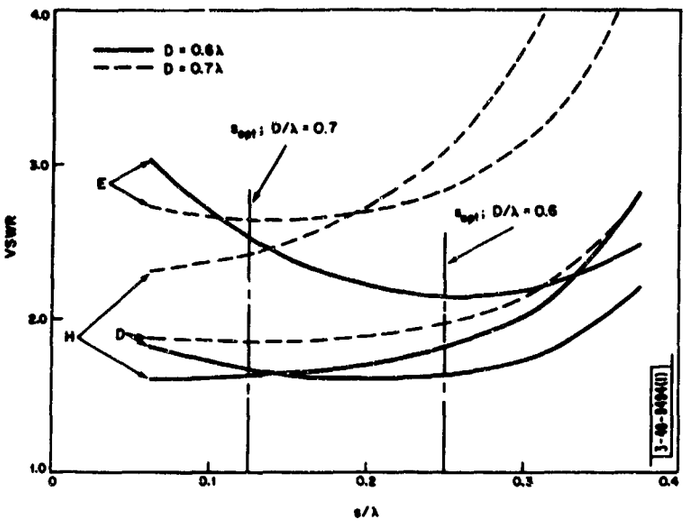

Fig. 15. VSWR at θ_{max} vs ground plane spacing for large, equilateral triangular-grid arrays of $\lambda/2$ dipoles.

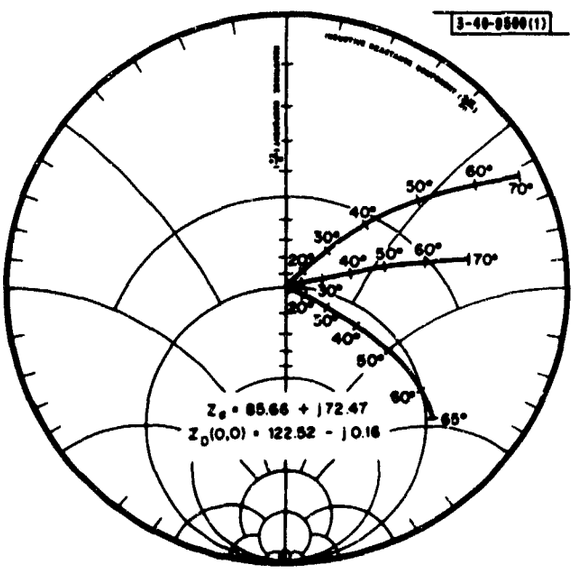

Fig. 16. Normalized impedance vs scan angle in E-, H-, and D-planes for a typical element of an equilateral triangular-grid array of $\lambda/2$ dipoles mounted 0.25 λ above ground plane; D = 0.6 λ.

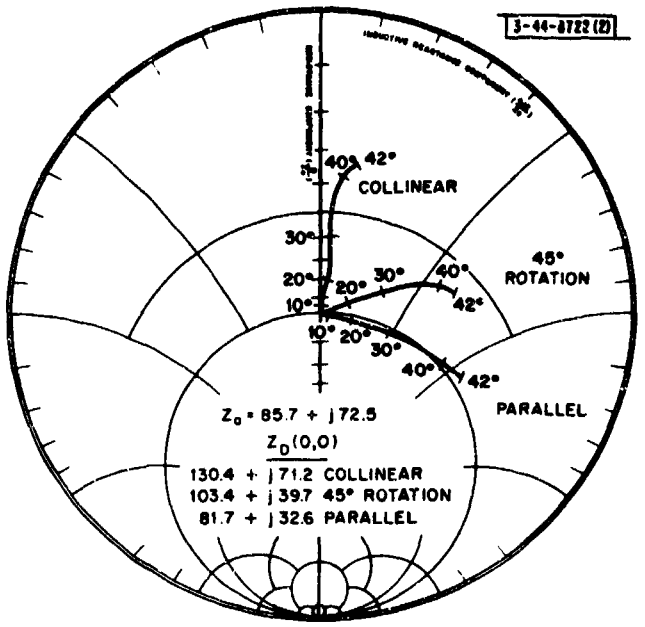

Fig. 17. Normalized impedance vs scan angle for typical elements in large, linear arrays of $\lambda/2$ dipoles mounted 0.25 λ above ground planes; D = 0.6 λ.

The relative impedance variation with scan angle is shown in Fig. 17 for a linear array of dipoles spaced 0.6 λ on centers, 0.25 λ above a ground plane for three orientations of the dipoles relative to the direction of the array. Observe that nearly pure resistance variation with scan angle is obtained when the dipoles are mounted collinearly, while for parallel dipoles, the variation is mainly reactive. Also note that the mismatch at the maximum scan angle is approximately the same for all three dipole orientations. Unfortunately, neither of these results applies for all ground plane and inter-element spacings; that is, the above choice of array parameters gives unique results and is presented merely to emphasize the different impedance behavior to be anticipated as a function of polarization in a linear array.

In Fig. 18, array performance is assessed as a function of inter-element and ground plane spacings (assuming a match at broadside) by giving the VSWR incurred at the maximum scan angle as a function of the spacings. From this figure, it is readily evident that a greater impedance variation with scan angle is exhibited by arrays of collinear dipoles for most ground plane spacings. The variation of maximum VSWR with ground plane spacing (up to s = 0.25 λ) is seen to be small for arrays of parallel and 45°-echelon dipoles.

If the frequency is now allowed to vary over a 20-percent band for an array with D = 0.6 λ and s = 0.25 λ, the impedance variation with scan angle at band center and at the band edges is as shown in Fig. 19. Results are given for collinear dipole and parallel dipole arrays. The fact that the impedance variation at the band edges is not substantially greater than at band center indicates that some other component (or components) in the feed network will probably limit the system bandwidth more than the antenna. (It is also interesting to observe that the Smith chart impedance plots for the parallel dipole and collinear dipole arrays remain approximately orthogonal as the frequency is varied.)

III. COUPLING IN REGULAR AND IRREGULAR FINITE ARRAYS

Intuitively, we would expect that the infinite array result discussed in the preceding section would accurately describe the impedance behavior to be expected for elements imbedded in even an irregular finite array, as long as the elements in the neighborhood of an element in question

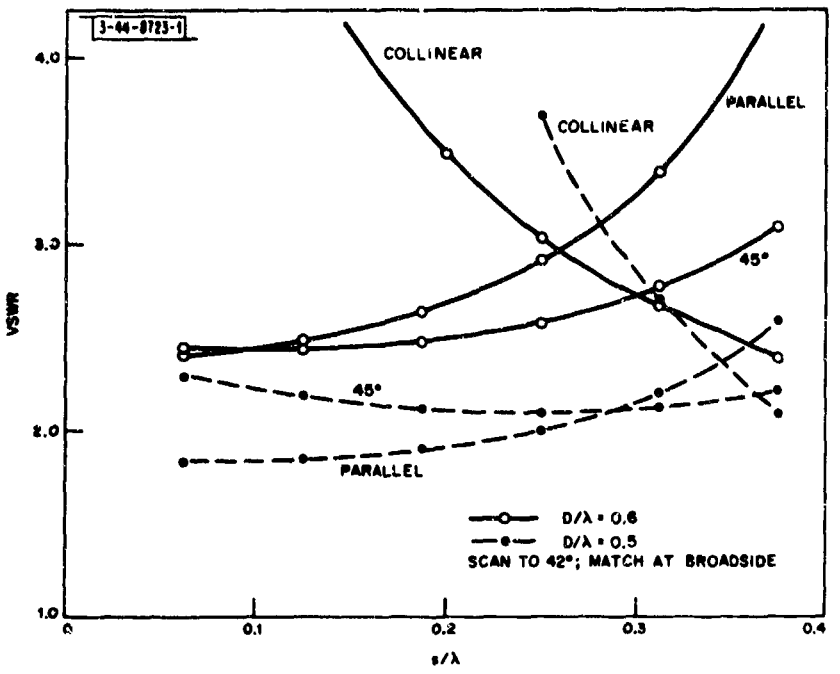

Fig. 18. VSWR at θ_{max} vs ground plane spacing for large, linear arrays of $\lambda/2$ dipoles.

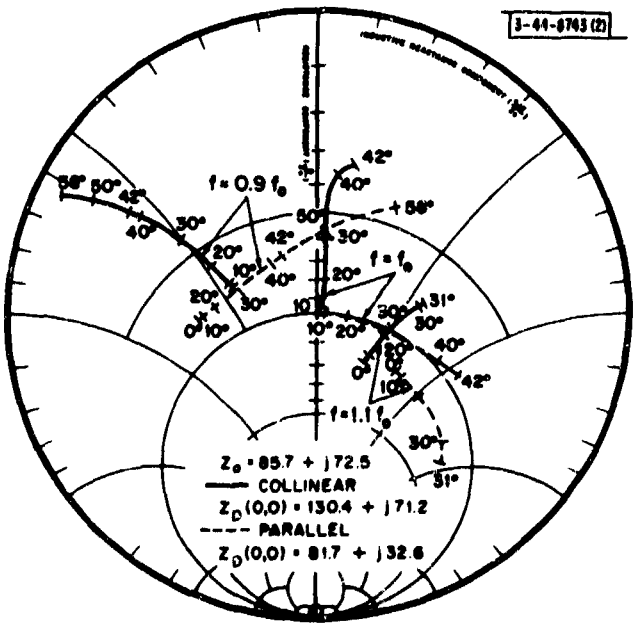

Fig. 19. Bandwidth behavior of the active impedance of elements in large, linear arrays of $\lambda/2$ dipoles; $D = 0.6\lambda_o$, $s = 0.25\lambda_o$.

provide a uniform environment; i.e., the element is not near the edge of the array and, if the array is irregular in spacing, the departure from regularity is small over a region of several elements. If this statement is to be useful, we must, of course, have quantitative data on the degree to which elements in nonuniform surroundings depart from the infinite array prediction. We shall see that this departure depends on the element details, the location of the other elements, and the feed network that is used to excite the elements.

Furthermore, we are now in a position to discuss the effects of coupling on array patterns (the patterns of infinite arrays are singularly uninteresting). Here again the nature of the element feed is important. For independently fed elements (separate excitation or an isolating feed network such as a well-matched corporate feed using four-port junctions), we can arrive at some very general results; for feed networks which allow element interaction through the feed, we can only outline a method of analysis and present some representative results for a few specific cases.

A. Methods of Analysis

Since the grating-lobe series can only supply an average (in the sense explained in Sec. II-D-3) element impedance behavior in a finite array, the first problem is to characterize the array (including mutual coupling) in a form suitable for mathematical analysis. This can be done by taking advantage of the well-known fact that the terminal currents and voltages of the elements in an array can be represented by circuit equations as Eq. (1), which is repeated here for reference:

$$V_{mn} = \sum Z_{mn,pq} I_{pq} \quad . \qquad \text{[Eq. (1)]}$$

Since there are N antennas, there will be N equations of the form of Eq. (1). This is analogous to the case of an N terminal-pair network. The set of equations can be written in the matrix form

$$V] = [Z]\, I] \qquad (21)$$

where V] and I] are N element column matrices, and [Z] is an $N \times N$ impedance matrix.

We could equally well relate I_{mn} to V_{pq} by an admittance matrix (inverse of [Z]) or relate incident and reflected waves by a scattering matrix. Of these, the scattering matrix is the easiest to measure in practice because it involves only a measurement of the power (magnitude and phase) coupled to antenna n when antenna m is driven with unit power. Measurements of impedance or admittance coefficients are generally much more difficult because they involve either open-circuit voltages or short-circuit currents.

None of the matrices is easy to compute theoretically for most types of array elements, because electromagnetic scattering (including multiple scattering), as well as induction and static field coupling, must be included in the computation of a single coefficient. However, dipoles of any length with infinitesimal diameters can be handled analytically by the induced emf method for computing mutual impedances.[15] The admittance and scattering matrices can then be computed from the impedance matrix. Figure 20 shows the behavior of the mutual impedances between $\lambda/2$ dipoles 0.25λ above ground as a function of relative position. Further data for dipoles and slots are given by Kraus.[15]

The second important part of the analysis of finite arrays is then the characterization of the network feeding the antennas. These feed systems can take any one of several forms, e.g., the

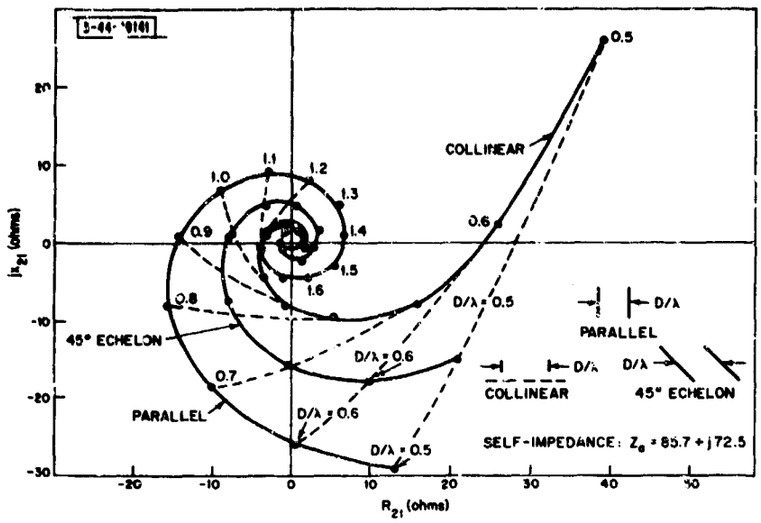

Fig. 20. Mutual impedance between λ/2 dipoles mounted 0.25 λ above ground plane as a function of relative position.

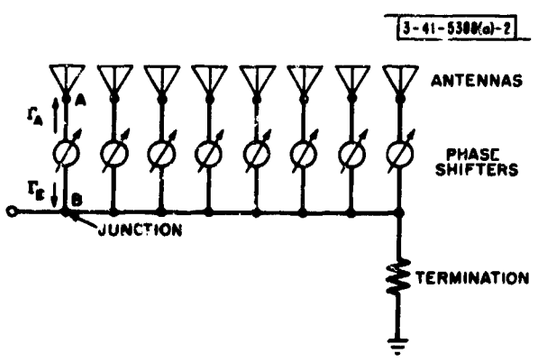

Fig. 21. Basic serial RF array feed with phase shifters in the branch lines.

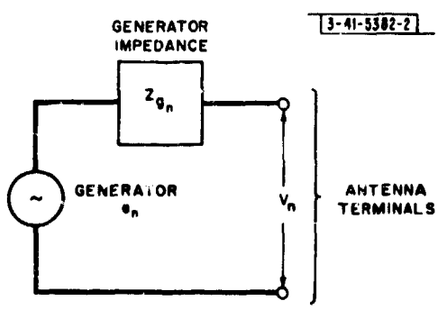

Fig. 22. Generator equivalent circuit for arrays with independent feeds.

serial feed of Fig. 21. Basically, they can be divided into two categories: independent (isolating) feeds and nonisolating feeds. An independent feed is one in which the feed to an antenna in the array is not influenced by the behavior of the remainder of the feed system except through radiation coupling between antennas. Examples of independent feeds are those constructed with directional couplers and those using circulators or isolators behind each antenna. A nonisolating feed, on the other hand, is one which does not meet the above criteria, that is, a feed network in which there is internal cross-coupling within the structure.

The independent source problem can most easily be analyzed directly from the impedance matrix by representing the sources as N independent generators with open-circuit voltages e_n and impedances Z_{g_n}, as indicated by the equivalent circuit of Fig. 22. The open-circuit voltages are assumed to have independently controllable amplitudes and phases. The terminal currents and voltages on the antennas are then related to the source parameters by

$$V_n = e_n - Z_{g_n} I_n \quad , \qquad n = 1, 2, \ldots N$$

or, in matrix form,

$$V] = e] - [Z_g] \cdot I] \tag{22}$$

where $[Z_g]$ is an $N \times N$ diagonal matrix with the diagonal terms given by the N generator impedances of the sources. When Eq. (22) is substituted in Eq. (1), we have

$$e] = \{[Z] + [Z_g]\} \cdot I] \quad . \tag{23}$$

Since the antenna currents are unknown, the impedance matrix, modified by the addition of the generator impedances to the antenna self-impedances, must be inverted to obtain an admittance matrix [Y] relating the antenna currents to the generator voltages

$$I] = [Y]\, e] \quad . \tag{24}$$

Once the currents have been computed for a particular set of drive voltages (a particular beam-pointing angle), it is a simple matter to compute the element driving impedance for any one of the antennas from

$$Z_{D_m}(\phi, \Theta) = \frac{e_m}{I_m} - Z_{g_m} \quad . \tag{25}$$

It should be recalled that for infinite arrays, we can rewrite Eq. (5) in terms of polar angles (see Fig. 3) as

$$Z_{D_{mn}}(\phi, \Theta) = Z_a + \sum_{p, q \neq m, n} Z_{mn, pq} \times \exp\{-jk[D_x(m - p) \sin\Theta \cos\phi + D_y(n - q) \sin\Theta \sin\phi]\} \tag{26}$$

where we generalize to a particular location $x = mD_x$, $y = nD_y$ for the element in question. From this equation, we have an alternate method to the grating-lobe series for computing the active impedance of an element in a very large, regular, uniformly illuminated array without resorting to a matrix inversion.

This approximation has been found to be extremely good for the center element in a large dipole array above a ground plane (the approximation is not as good when the ground plane is

absent). In fact, the active impedance of the center element in a 65 (collinear) × 149 (parallel) array (with a ground plane) agrees within 0.1 percent with that of an infinite array, except near endfire. For this reason, we often use the 65 × 149 array results instead of the corresponding (and nearly identical) infinite array results.

Nonisolating feeds can be represented by an (N+M) × (N+M) scattering matrix $[S_F]$, where N is the number of antenna ports and M is the number of input ports. This scattering matrix can be written in partitioned form as

$$[S_F] = \left[\begin{array}{c|c} \underline{S}_{11}^F & \underline{S}_{12}^F \\ \hline \underline{S}_{21}^F & \underline{S}_{22}^F \end{array}\right] \tag{27}$$

where $\underline{S}_{11}^F$ is an M × M matrix which represents the input mismatches and cross-couplings among the input lines, $\underline{S}_{21}^F$ is an N × M matrix representing the coupling from the input ports to the antenna ports (the antenna illumination under matched conditions), and $\underline{S}_{22}^F$ is an N × N matrix giving the output mismatches (looking back at the feed) and the output cross-couplings among the feed lines. When only reciprocal devices are used in constructing the feed, $\underline{S}_{12}^F$ will be just the transpose of $\underline{S}_{21}^F$. Also, the feed scattering matrix will be unitary (the inverse of $[S_F]$ is given by the transpose-conjugate of $[S_F]$), if the components in the feed are lossless.

Thus, for a particular feed network, the characteristics of the components which comprise the network can be combined to obtain a scattering matrix in the form of Eq. (27). Specific examples are treated in Sec. III-C. In general, we can state that the performance of these nonisolating feed systems is quite sensitive to the design parameters of the network (principally line lengths) because of multiple reflections within the structure. These reflections can add vectorially at the various ports to give either very good or very poor array illumination depending on the particular design of the network.

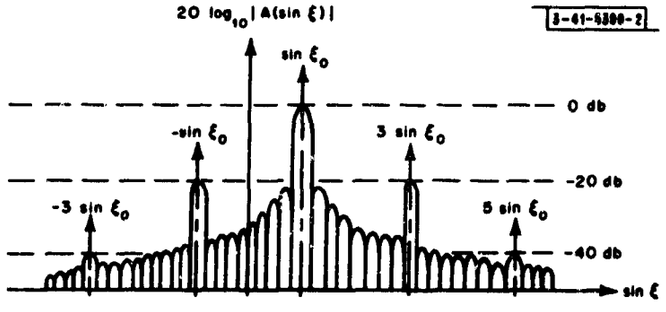

Fig. 23. Typical array function showing spurious lobes for $|\Gamma_A \Gamma_B| = 0.1$ for an array using three-port junctions.

The phase shifters used in the composite system (antennas, feed network, and phase shifters) can also have a strong influence on the array illumination. For example, when reciprocal phase shifters are used, the part of the wave reflected from an antenna that is reflected back to the antenna by the feed network generates a spurious beam in a different direction, resulting in a high sidelobe in the array pattern,[16] as indicated in Fig. 23. Quantitatively, for any feed with reflection coefficient Γ_A looking into the antennas and Γ_B looking into the feed (see Fig. 21), the illumination coefficients are related to the original coefficients $a_n \exp[-jnkD \sin\Theta]$ by

$$a_n' = a_n \sum_{q=0}^{\infty} (-1)^q (\Gamma_A \Gamma_B)^q \exp[-jnkD(2q+1)\sin\Theta] \quad . \tag{28}$$

Thus, for a reflection coefficient product of magnitude 0.1, the resultant far-field pattern would be approximately as shown in Fig. 23 for a phase shift setting corresponding to a three-beamwidth pointing angle from broadside. On the other hand, when nonreciprocal phase shifters are used, the re-reflected waves arrive back at the antennas with the same relative phase shifts as the primary waves and hence, to a first order, only affect the amplitude (gain) of the array pattern.

B. Arrays Fed by Independent Sources

In this section, we examine some small-array configurations to determine (1) the correlation of finite and infinite array element impedance and element gain properties and (2) the magnitude and extent of edge effects in small arrays.

1. Impedance Behavior of Linearly Polarized Arrays

For these investigations, we will restrict ourselves to 7 × 9 and 9 × 11 arrays. (The impedance matrix for a 9 × 11 array is the largest which can be conveniently handled within the core storage of an IBM 7094 digital computer.) The geometry and element numbering system we will adopt for a 9 × 11 rectangular-grid array are shown in Fig. 24. Alternate rows of the array are offset by $D_x/2$ to obtain the triangular-grid array discussed later.

The impedance variation with scan angle for the center element of a 7 × 9 array of λ/2 dipole radiators above a ground plane ($D_x = D_y = 0.5\lambda$, $s = 0.25\lambda$) is shown in Fig. 25. One set of curves

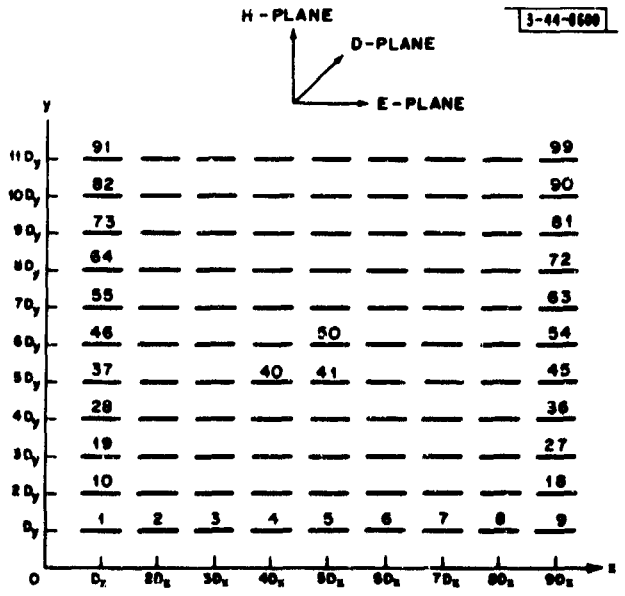

Fig. 24. Geometry and element numbering system for a 9 × 11 element array configuration (element 50 is the center element for this array).

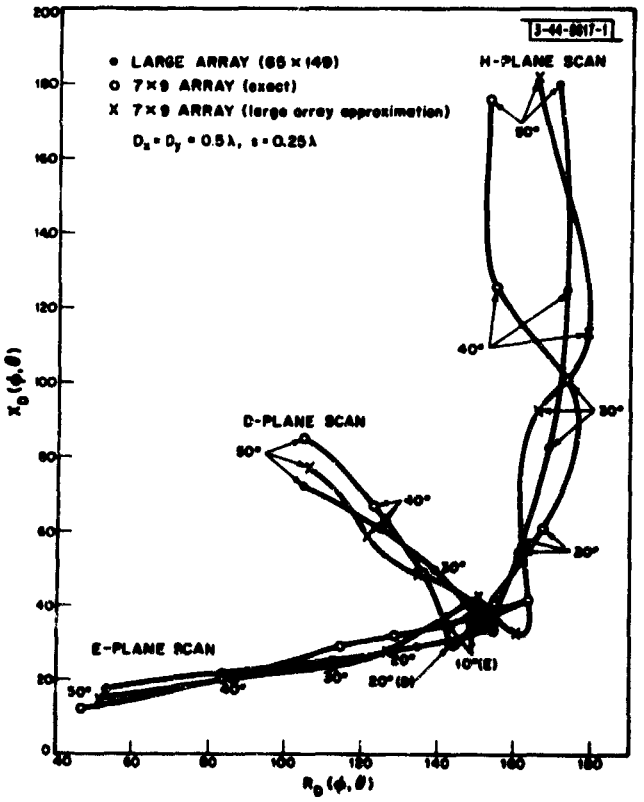

Fig. 25. Comparison of impedance variation of the center element in a 7 × 9 array of λ/2 dipoles with that of an infinite array.

gives the results for the exact, matrix inversion solution, while another set gives the results obtained with the approximation of Eq. (26). Both sets of curves are then compared with the impedance variation of a large array (65 × 149) with the same geometry. It is evident that the 7 × 9 array results (both exact and approximate) agree reasonably well with the large-array results in all three scan planes (the difference in the magnitudes of the 7 × 9 array impedance and the large-array impedance at a particular scan angle is less than 14 percent). Near broadside, the small-array impedances exhibit rather unusual behavior, while at larger scan angles, they tend to oscillate around the values for a large array. An increase in array size to 9 × 11 results in a somewhat better approximation to an infinite array, but the deviations in the magnitude of the impedance compared to the large array are still of the order of 10 percent. A still better approximation to the infinite array impedance variation can be found by taking the geometric mean of the 7 × 9 and 9 × 11 impedances at each of the scan angles.[17]

Similar results are observed when the arrays have triangular grids as shown in Fig. 26. In this figure, the impedance variation with scan angle of a central element of a 9 × 11 equilateral triangular-grid array (D = 0.6 λ, s = 0.25 λ) is compared to that of a corresponding infinite array for three scan planes. Again it is found that the error in approximating the impedance behavior of a large array by a small array is only about 10 percent. The small-array impedance variation oscillates around that of an infinite array which is again just typical of the behavior expected when a function is approximated by a truncated Fourier series.

The small-array behavior differs more markedly from that of an infinite array when the ground plane is removed, as evidenced by Fig. 27 where the impedance variation of the center element in 7 × 9 and 9 × 11 arrays is compared. It is clear from the very poor correlation

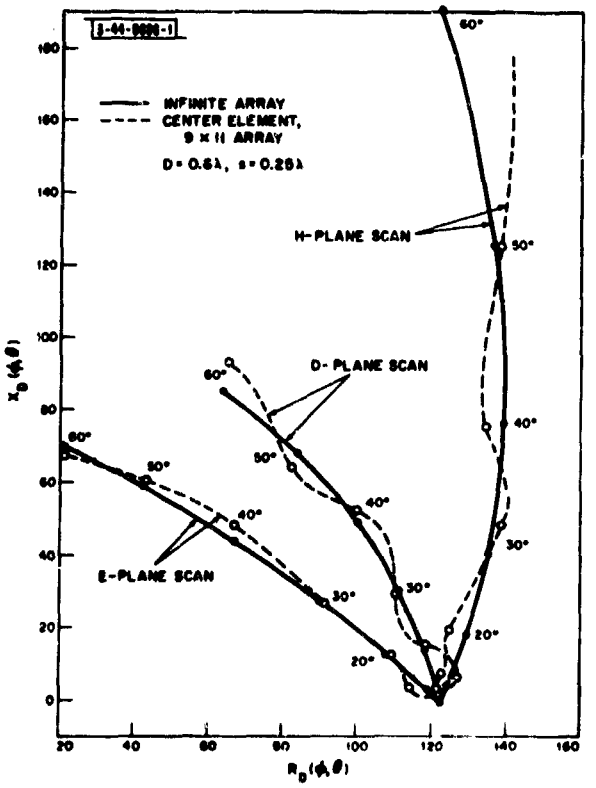

Fig. 26. Comparison of impedance variation of the center element in a 9 × 11 equilateral triangular-grid array of λ/2 dipoles with that of an infinite array.

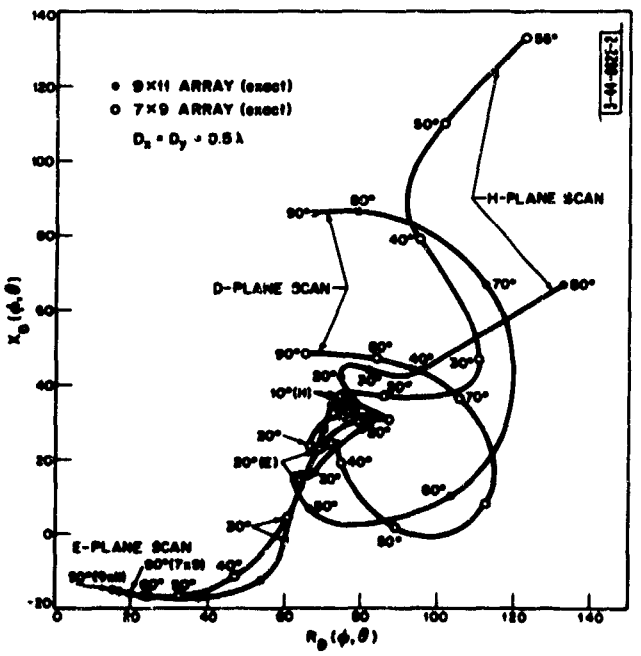

Fig. 27. Comparison of impedance variation of the center element in 7 × 9 and 9 × 11 square-grid arrays of λ/2 dipoles without ground planes.

between the two array impedance variations that small arrays of dipoles without a ground plane or slots in a ground plane are not very useful for predicting the performance of large arrays.

As discussed above, the impedance variation (magnitude) with scan angle for the center element (No. 50 of Fig. 24) of a 9 × 11 square-grid array agrees within about 10 percent with the values for an infinite array. For the impedance variation with scan angle of an interior, non-center element, there is still reasonably good agreement with an infinite array, even though there may be substantial asymmetry in a given scan plane: for a particular scan plane specified by $\phi = \phi_i$, the impedance variation with scan angle Θ for one direction of scan from broadside will differ from that when the beam is scanned in the opposite direction $Z_{D_m}(\phi_i + \pi, \Theta) \neq Z_{D_m}(\phi_i, \Theta)$.

The situation is considerably worse when the elements are on the edges of the array as shown in Fig. 28 for the element (46) in the middle of the edge where the dipoles are parallel, and in Fig. 29 for the element (5) in the center of the edge where the dipoles are collinear. In these figures, it is observed that the correlation of the impedance variation with that for an infinite array is very poor. In addition, there is considerable asymmetry as evidenced by the fact that $Z_{D_m}(\phi_i + \pi, \Theta)$ differs markedly (in magnitude and phase) from $Z_{D_m}(\phi_i, \Theta)$. Note that the array is symmetrical about element 46 for H-plane scan, and therefore no asymmetry is observed in the H-plane impedance variation with scan angle, as shown in Fig. 28. Similarly, the array is symmetrical about element 5 for E-plane scan.

From these results, we conclude that for a 9 × 11 (or smaller) array, there is, strictly speaking, no typical element; that is, every element has a different impedance variation with scan angle. However, for dipoles above ground, the center element and the edge effects computed or measured for the small array would give a reasonable indication of those to be expected in a large array. For dipoles without a ground plane, slots in a ground plane or open waveguides, the 9 × 11 array gives only rough qualitative estimates of large-array behavior.

2. Pattern Behavior of Regular Linearly Polarized Arrays

Since we can model the excitation of a typical element of an independently fed array by a circuit such as that of Fig. 22, we can conceptually turn on each generator of the array individually, with the others turned off ($e_m = 0$, $m \neq n$). When the generators are shut off, all passive elements are effectively terminated in an impedance Z_g. With only $e_n \neq 0$, a current i_n will flow past some reference point on antenna n, directly exciting antenna n and parasitically exciting the rest of the array through mutual coupling. A measurement of the far field under these conditions produces some relative field strength which we will call $\bar{f}_n(\phi, \Theta)$, since it is due to the n^{th} element generator. The experiment can be repeated for each element, and the far field can be found by taking the vector sum of the individual element contributions, properly weighted by a phase term dependent on the element location

$$\bar{F}(\phi, \Theta) = \sum_n \bar{f}_n(\phi, \Theta)\, i_n \exp[jk\bar{\rho}_n \cdot \bar{e}_R] \tag{29}$$

where $\bar{e}_R$ is a unit vector in the direction of the observation point, and $\bar{\rho}_n$ is a vector from the origin to the n^{th} element location. For completely arbitrary distributions of elements, little more can be said. However, for the important case in which (a) the array is large compared to the region over which element interaction is strong so that edge effects can be neglected, (b) the

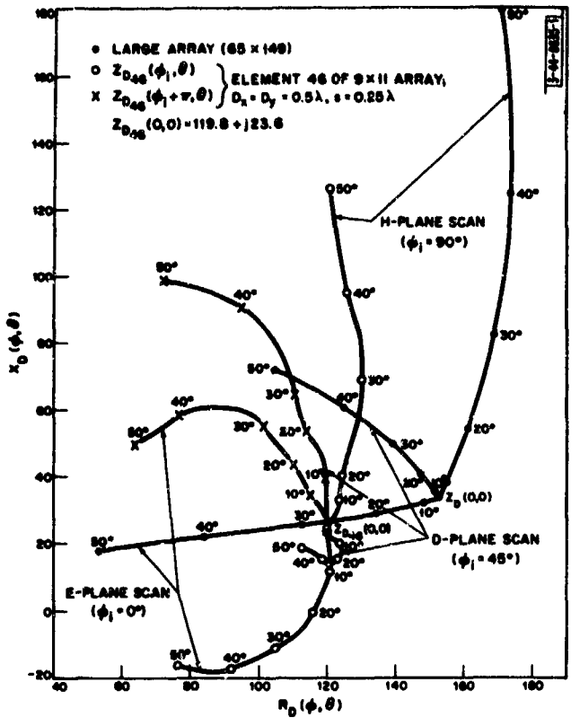

Fig. 28. Comparison of impedance variation of the element in the center of the parallel dipole edge of a 9 × 11 array of λ/2 dipoles with that of a large array.

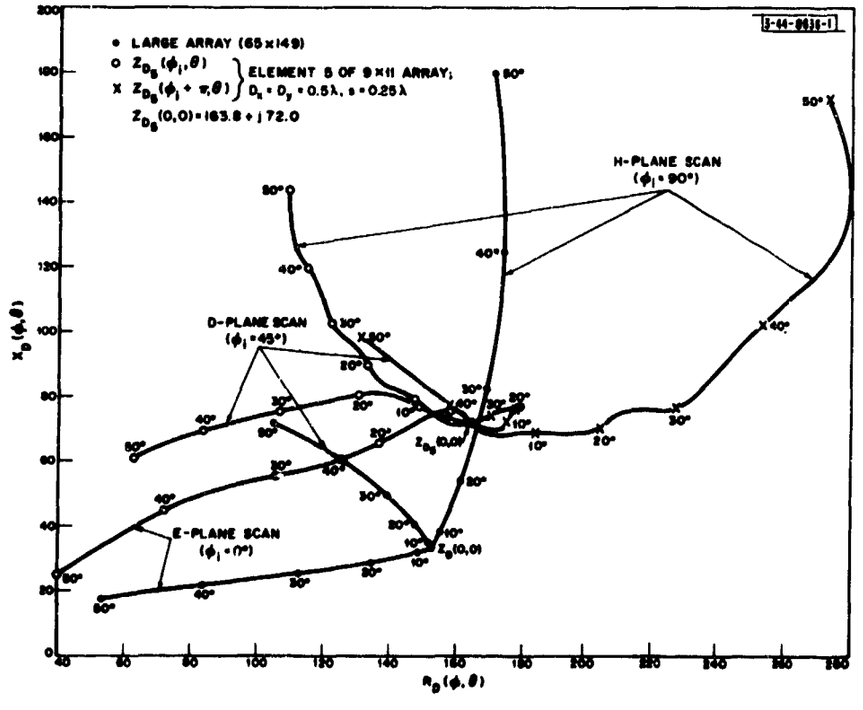

Fig. 29. Comparison of impedance variation of the element in the center of the collinear dipole edge of a 9 × 11 array of λ/2 dipoles with that of a large array.

elements and their generator impedances are nominally identical, and (c) the elements are regularly spaced on a flat† surface so that all interior elements "see" the same interaction environment, the pattern of each element, measured as indicated above, will be essentially the same as the pattern of any other element. We can then factor Eq. (29) and write

$$\bar{F}(\phi, \Theta) = \bar{f}(\phi, \Theta) \sum_n i_n \exp[jk\bar{\rho}_n \cdot \bar{e}_R] \tag{30}$$

where $\bar{f}(\phi, \Theta)$ is a typical $\bar{f}_n(\phi, \Theta)$.

The factor $\bar{f}(\phi, \Theta)$ multiplying the summation in Eq. (30) is the pattern of a typical (central) element in the presence of all the other elements when they are terminated in the impedance from which they are nominally excited, and is usually referred to as the "element factor." The i_n of Eq. (30) represents the current flow in the n^{th} element due solely to the excitation of its own generator. For all elements (neglecting edge effects), i_n is related to e_n of Fig. 22 by the same proportionality independent of the other element excitations, and we could replace i_n by e_n in Eq. (30), except for a scale factor which is the passive element driving impedance.

The practical significance of this development lies in the fact that the summation of Eq. (30) is exactly the array factor of an array of isotropic radiators, the properties of which have been extensively discussed. The element factor contains essentially all the pattern effects of the element type and the interaction between elements. The pattern of the entire array when only one element is excited and the others terminated is much broader than the pattern when the entire array is excited; hence, $\bar{f}(\phi, \Theta)$ is a function whose variation with angle is slow compared to any reasonably directive array factor in large arrays. The patterns are qualitatively similar to those of Fig. 30. The element factor acts as a window of varying degrees of opaqueness through which the array factor "looks." We can qualitatively conclude that under normal circumstances, in large arrays, the element factor structure will have little effect on the relative structure of the main beam and close-in sidelobes of a large array. However, in arrays in which the beam is scanned by element phasing, the absolute strength of the pattern will be varied with angle to conform to the element factor weighting, since the scanning moves the array factor in space while the element factor is stationary, as indicated by Fig. 30.

For elements in which mutual impedances can be analytically determined, the computation of the element factor is straightforward. Perhaps more important, in the frequent case of elements for which computational formulas do not exist, the element factor can be determined experimentally by building an array only large enough to render edge effects negligible on the pattern of the central element. Finally, we can also rationalize some generally valid, quantitative conclusions about element factor shapes.

Of course, if the antenna elements are separated far enough so that the interactions are negligible, the $\bar{f}_n(\phi, \Theta)$ become the patterns of isolated elements (which are given in the literature for a wide variety of radiators). However, only when the elements are separated by distances that are much greater than their largest dimension is it safe for us to assume that interaction effects are negligible. Unfortunately, achieving freedom from interaction in this way results in spacing the elements sufficiently far apart that several grating lobes of the array factor appear in visible space, as indicated in Sec. II-D.

† The modification for large, regularly spaced arrays on curved surfaces with large radii of curvature (compared to λ) is tedious, but not conceptually difficult.

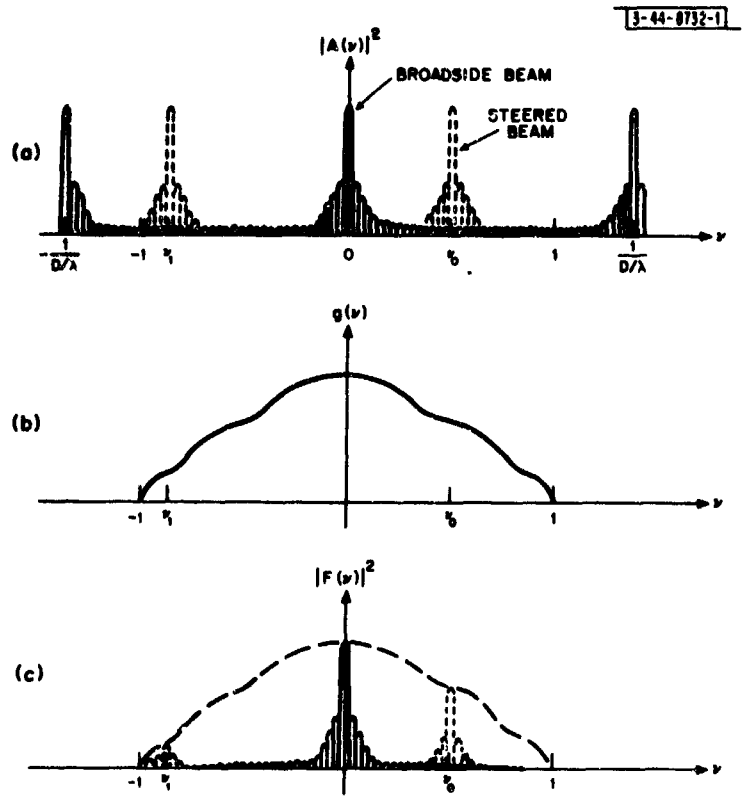

Fig. 30. Qualitative relationship between element gain function and array factor (ξ = angle from broadside): (a) array factor, (b) element gain function, (c) resulting pattern.

The more interesting case for many array applications is that of closely spaced elements – in particular, the case of only slightly directive elements spaced less than a wavelength on centers. Here some element factor shapes can be inferred from a consideration of the gain and directivity variation of electronically scanned arrays.

The array gain G is a measure of efficiency of the array in using all the energy available, and involves questions of array impedance matching and ohmic losses. Although mismatch effects are not always included as a factor in the gain of an antenna, they will be included in this discussion. Such effects are taken into account by defining the gain as the ratio of power density per unit solid angle at the peak of the main beam to the power density that would be achieved by radiating all the available power isotropically.† For a large, flat, equally spaced array of identical radiators, it is a simple matter to determine the gain as a function of scan angle in terms of the element factor shape.

The power density per unit solid angle is

$$P(\phi_o, \theta_o) = |B|^2 |f(\phi_o, \theta_o)|^2 \left| \sum_n e_n \right|^2$$

where B is an angle invariant factor, the value of which will be seen to be immaterial. The power available from each generator, assuming that the equivalent circuit of Fig. 22 applies, is

† The IEEE Standards defines gain as relative to the total power into the antenna, ignoring unmatched effects. The definition of gain used herein thus differs from the standard definition by the factor $1 - |\Gamma|^2$.

$|e_n|^2/4R_g$, where $R_g = R_e(Z_g)$, and we assume all element drives have the same impedance. Hence, the total power available to the array is $\sum_n |e_n|^2/4R_g$ from which it follows that the gain of an array is

$$G(\phi_o, \theta_o) = (4\pi)\,|B|^2\, 4R_g |f(\phi_o, \theta_o)|^2 \frac{\left|\sum_n e_n\right|^2}{\sum_n |e_n|^2} \quad .$$

Note that if we drive only one element in the array, the gain of that element is given by

$$g(\phi_o, \theta_o) = (4\pi)\, 4R_g |B|^2\, |f(\phi_o, \theta_o)|^2 \quad .$$

Further, if $e_n = 1$, for all n, then

$$\frac{\left|\sum_n e_n\right|^2}{\sum_n |e_n|^2} = N$$

where N is the number of elements in the array. For arbitrary taper, we can define a taper efficiency η by

$$\frac{\left|\sum_n e_n\right|^2}{\sum_n |e_n|^2} = \eta N \quad .$$

Comparison of the relationships for G, g, and ηN gives the simple result

$$G(\phi, \theta) = g(\phi, \theta)\, \eta N \quad . \tag{31}$$

The factor $g(\phi, \theta)$ is referred to as the "element gain function," and its spatial variation with the beam-pointing angles ϕ and θ is $|\bar{f}(\phi, \theta)|^2$. Equation (31) is the quantitative statement of the fact that the element factor acts as a weighting function on the field strength of the array. It is easily established that the directivity of a planar array of N_a active radiators with no visible grating lobes is

$$U(\theta) = 4\pi\eta\, \frac{N_a}{\lambda^2}\, a \cos\theta \tag{32}$$

where θ is the angle from the array broadside direction, and a is the area allotted to each element. For independently excited radiators with no ohmic loss, which can support only a single polarization, the array directivity and gain as defined herein can differ only as the result of mismatch losses. These losses can be taken into account, in terms of the voltage reflection coefficient $\Gamma(\phi, \theta)$ seen when looking into a typical element when the entire array is excited, by writing

$$G(\phi, \theta) = U(\theta)\, (1 - |\Gamma(\phi, \theta)|^2) \quad .$$

Substitution of Eq. (32) into this expression sheds some light on the element factor behavior to be expected as a function of element spacing:

$$g(\phi, \theta) = 4\pi\, \frac{a}{\lambda^2} \cos\theta\, (1 - |\Gamma(\phi, \theta)|^2) \quad . \tag{33}$$

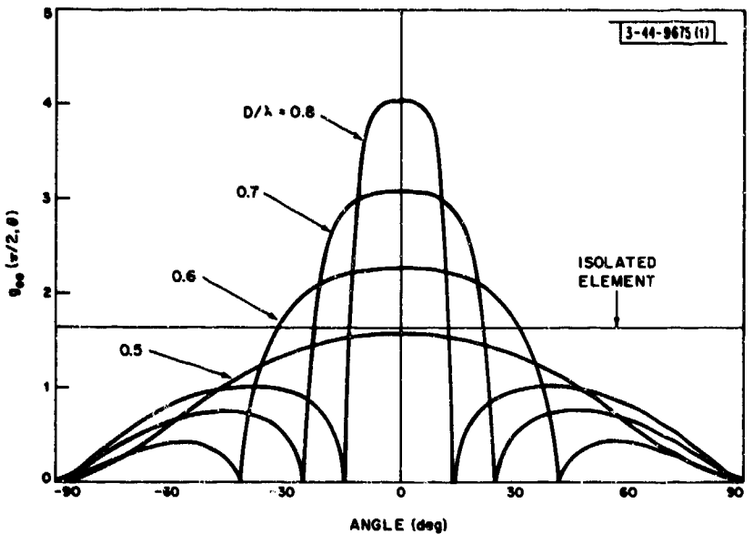

Fig. 31. H-plane element gain functions for arrays of λ/2 dipoles without ground planes.

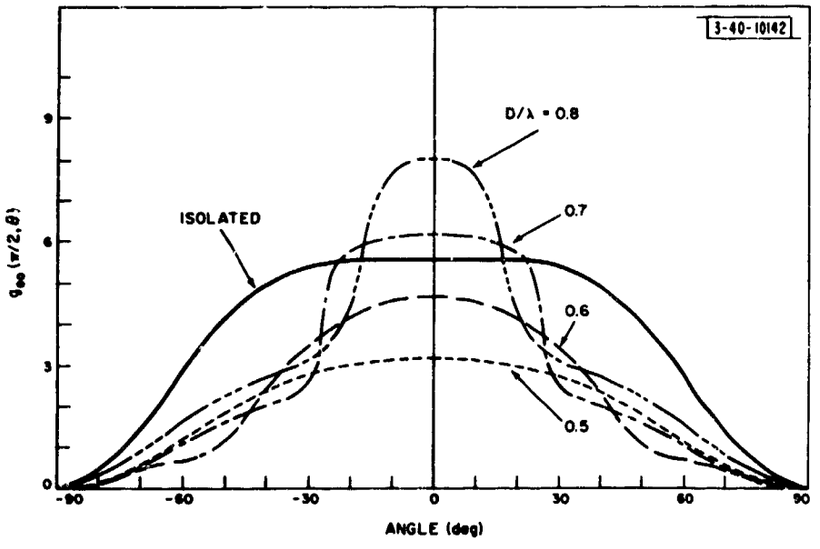

Fig. 32. H-plane element gain functions for arrays of λ/2 dipoles mounted 0.25 λ above ground planes.

We can now draw some inferences about the general nature of the gain function shapes to be expected in planar arrays.†

The only place the type of radiator enters the above expression is implicitly in $\Gamma(\phi, \Theta)$. Regardless of the type of radiator, we can choose the generator impedance to match the element at some angle of scan of our choice. If, for the sake of illustration (and maximum broadside gain), we match the elements when the array is phased for a broadside beam, we can make the following generalization about the element pattern for small (less than a wavelength in dimension) elements from Eq. (33). As we space the elements farther apart, the value of $g(0, 0)$ can be made to increase directly with the area per element if the proper generator impedance is chosen for each spacing. However, as the element spacing is increased, the angles at which grating lobes become visible decrease. At these angles, the array directivity must drop rapidly by approximately 3 db, and the gain function must behave in a similar fashion (we are not matched at these angles, so only approximate statements are justified). That the element pattern does behave in such a manner has been verified analytically for some elements and experimentally for many others. Figure 31 shows element patterns of the center element of an array of dipoles without a ground plane for various spacings on a square element grid, and Fig. 32 shows similar data for dipoles $0.25\,\lambda$ above a ground plane. The figures illustrate the effects stated.

If the elements are not matched to maximize $g(0, 0)$ for each spacing, the result is a decrease in broadside gain and, usually, a slight increase in the width of the element factor main lobe. For example, a convenient generator impedance choice from a practical standpoint is to match the impedance of a single isolated antenna (with ground plane, if used). Indeed, Eq. (5) indicates that for an essentially infinite array scanned over all phasings (including those producing grating lobes), the <u>average</u> driving impedance is just

$$\int_{-\pi}^{\pi}\int Z_D(\alpha, \beta)\, d\alpha\, d\beta = Z_{oo,\,oo} \tag{34}$$

which is essentially the same as the impedance of an isolated element for many practical types. Consequently, this choice comes close to minimizing the maximum impedance variation, and will usually produce a match at some scan angle other than broadside. The resulting element gain function is usually "saddle-shaped" as indicated in Fig. 33.

For arrays on curved surfaces, if the curvature is shallow compared to the extent over which appreciable coupling takes place, the element gain function shape relative to each element's own broadside angle will be similar to those of an equivalently spaced planar array. Thus, even though Eq. (30) fails to apply, the element patterns can usually be taken into account in a straightforward and relatively simple manner.

The element gain function concept has both practical and fundamental significance. It is a practical way to assess the gain-vs-scan-angle performance of a large array by using a small or modest array without the requirement of a complex feed system. We need only construct an array large enough so that the central element "sees" negligible edge effects (how large in each dimension depends on the rate of decay of coupling for the particular element in the direction in

† Equation (31) applies also to linear arrays; hence, a dependence analogous to Eq. (33) of the gain function of an element in a linear array on element spacing can be made (see Fig. 43), but the result is complicated by the fact that the variation of array gain with scan angle depends on the element pattern in the plane orthogonal to the array.

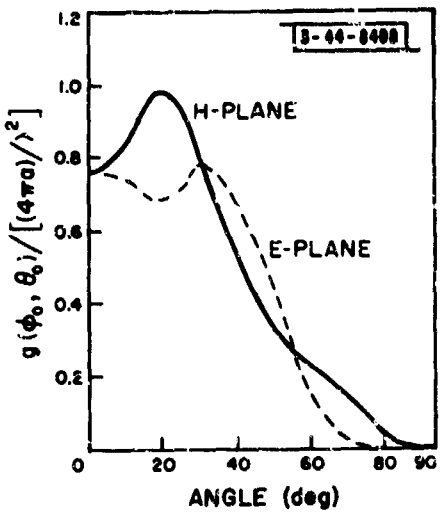

Fig. 33. Principal plane gain functions for a $\lambda/2$ dipole in an array; generator matched to the impedance of an isolated element.

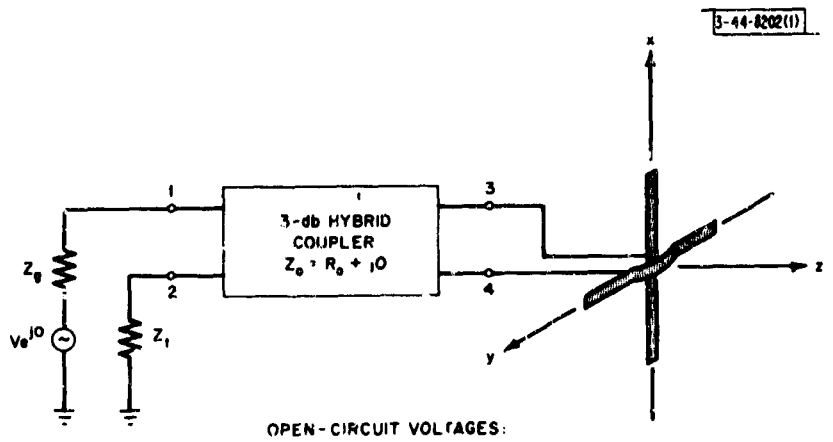

OPEN-CIRCUIT VOLTAGES:

$$V_{oc}^{3} = \frac{V}{\sqrt{2}} e^{j0}$$

$$V_{oc}^{4} = \frac{V}{\sqrt{2}} e^{-j\pi/2}$$

Fig. 34. Hybrid-fed, crossed-dipole-pair element configuration; typically, $Z_g = Z_t = Z_0$.

question, as elaborated on previously). All elements are then terminated except the central element, and a pattern is taken. Experiments in design parameters can be conducted on a limited model.

There is also a connection between the shape of the element gain function and the complex driving impedance of the elements.[18] For example, note that in an essentially infinite array for which the elements have a voltage reflection coefficient behavior $\Gamma(\phi, \Theta)$, the current into an element at scan angle ϕ, Θ is $1 - \Gamma(\phi, \Theta)$. Furthermore, the shape of the element gain function can be used to demonstrate a fundamental limitation on the average reflected power over all phasings, applicable to any element.[1]

3. Gain, Polarization, and Impedance Properties of Independently Fed Circularly Polarized Arrays

An additional effect of element interaction on array patterns is found in arrays of elements which can support more than one polarization. The general effect of the coupling is to cause the array polarization to vary with scan angle in a manner dependent on all the factors that enter into the determination of coupling effects: element type, feed circuit details, and element grid shape and spacing.

To illustrate these effects, we present in this section some results of an analysis of arrays of elements made of crossed dipoles. In particular, we examine arrays of such elements driven through a hybrid power divider as indicated in Fig. 34, so that the elements can be considered independently excited. In such a case, an element gain function for a dipole pair in the array can be defined in the same manner as for linearly polarized arrays in the previous section. However, there are contributions to the gain function from both co-directed and orthogonally directed dipoles, and hence the gain function must be defined relative to some polarization vector $\overline{e_p}$:

$$g(\phi, \Theta, \overline{e_p}) = \frac{2\pi}{R_o} \left| (\overline{e_p} \cdot \overline{e_x})\, f_i^x(\phi, \Theta)\, [1 - \Gamma^x(\phi, \Theta)] - j(\overline{e_p} \cdot \overline{e_y})\, f_i^y(\phi, \Theta)\, [1 - \Gamma^y(\phi, \Theta)] \right|^2 \tag{35}$$

for an interior element of a large array, where $f_i^x \overline{e_x}$ is the vector element pattern of the x-directed elements, and $\Gamma^x(\phi, \Theta)$ is the reflection coefficient looking into those elements, and similarly for the y-directed elements. It is readily shown that for an infinite, regularly spaced array above a ground plane, the broadside gain relative to a right-circular sampling polarization vector is

$$g(0, 0, \overline{e_r}^*) = 4\pi \frac{a}{\lambda^2}$$

when all dipoles are matched to the feed hybrid at broadside [$R_o = R_D^x(0, 0) = R_D^y(0, 0)$], a result expected on the basis of directivity considerations.

From Eq. (35), it is possible to derive expressions for the gain relative to right-circular, left-circular, or any arbitrary linear sampling polarization vector at any scan angle. These relations can then be used to determine the characteristics (ellipticity, tilt angle, left- and right-circular gain, etc.) of the wave transmitted in any direction.

In order to assess the effects of an array environment on the dipole gain and impedance, we first consider an isolated dipole pair. The polarization of the transmitted wave at various points in space is the characteristic of importance for the isolated element. A typical power pattern as would be measured by a spinning, linearly polarized receiving dipole is shown in Fig. 35 for a

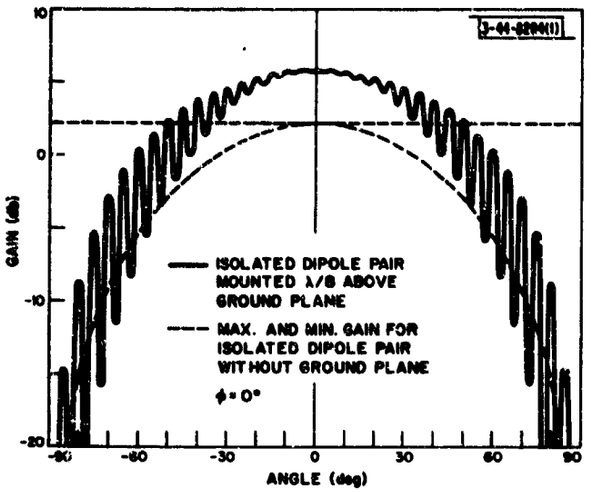

Fig. 35. Isolated dipole-pair gain functions.

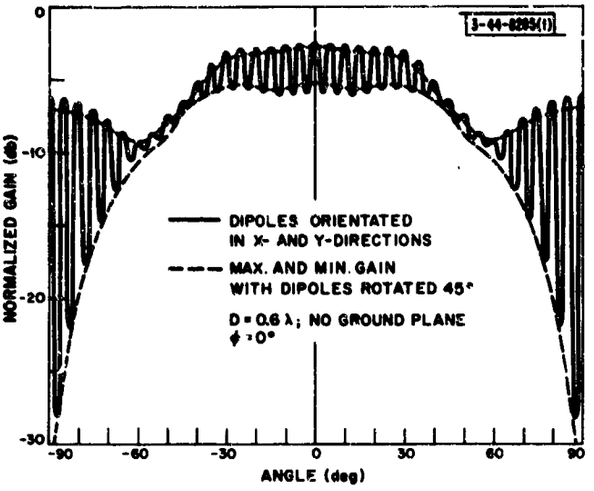

Fig. 36. Gain function of center element of seven-element linear array of hybrid-fed, crossed-dipole pairs.

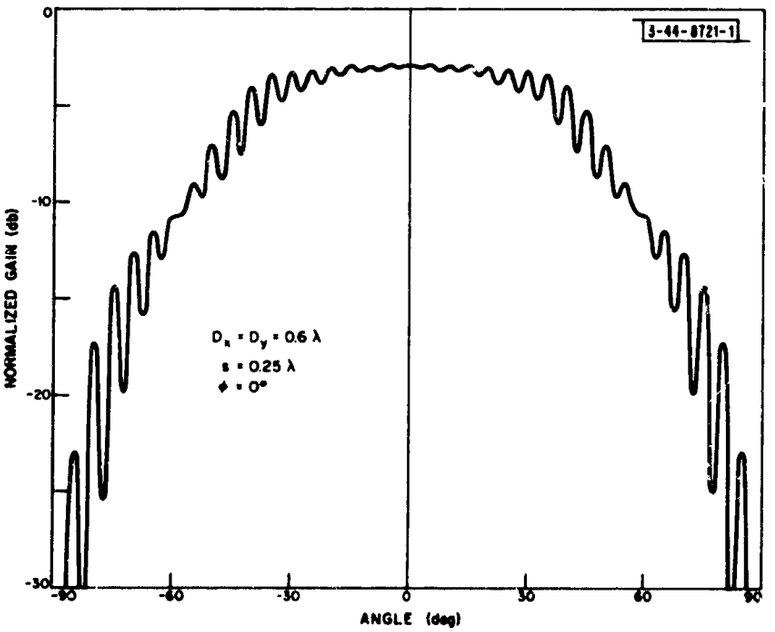

Fig. 37. Gain function of center element of 13 × 13 array of hybrid-fed, crossed-dipole pairs.

dipole pair above an infinite ground plane. Also shown are the maximum and minimum bounds of the corresponding pattern for a crossed-dipole pair at any point in space.

When seven elements are arranged in a linear array (no ground plane), the polarization characteristic of the gain function for the center element is as shown in Fig. 36 for a cut in the direction of the array when the dipoles are matched to the feed circuit at broadside and the fourth port of the hybrid (Fig. 34) is terminated in a matched load. Note that the array environment has substantially changed the gain from that of an isolated element, with the result that nearly circular polarization is obtained at a scan angle of 45°, while at broadside the polarization ellipse axial ratio (max. gain/min. gain) is about 3 db. (This is similar to the results observed by Parad and Kreutel[19] for a seven-element hexagonal array of circular waveguides.) The polarization characteristic can be improved only slightly by rotating the elements 45° as demonstrated by the dashed curves in Fig. 36. Note that the polarization of the transmitted wave at broadside is elliptical even with the dipoles rotated.

As a final result, we consider the center element of a 13 × 13 square-grid array above a ground plane. A principal plane (ϕ = 0°) gain pattern as would be measured by a spinning, receiving dipole when the elements are matched for broadside radiation and the fourth port is terminated is shown in Fig. 37. For this array, perfect, right-circular polarization is obtained at broadside even in the presence of mutual coupling. This is a consequence of the complete symmetry of the array about the center element. The polarization properties in other planes of scan for this array are shown in Fig. 38, where the polarization ellipse axial ratio variation with scan angle for both an isolated dipole pair and the center dipole pair in the 13 × 13 array is plotted. Note that the array environment can substantially alter the polarization of the transmitted wave (as compared to that of an isolated dipole pair) and can in fact improve the circularity of the radiated wave for optimum ground plane spacing ($s \approx 0.25\lambda$ for $D_x = D_y = 0.6\lambda$). Since the center element of the 13 × 13 array "sees" an environment which is approximately the same as that seen by an element in an infinite array, the polarization results given in Fig. 38 should be quite indicative of large-array polarization variation with scan angle to be expected from an array of

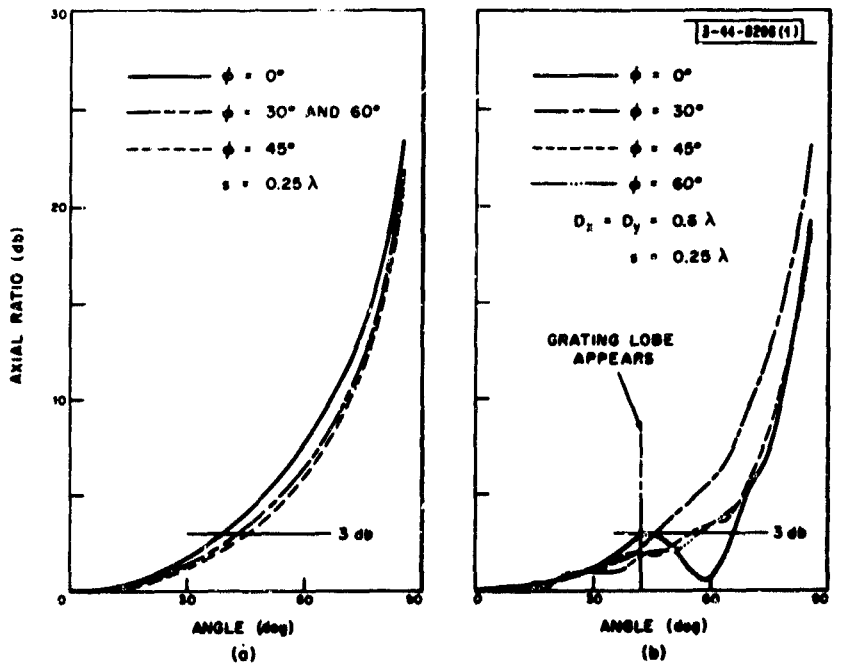

Fig. 38. Polarization ellipse axial ratio: (a) isolated element, (b) center element in 13 × 13 array.

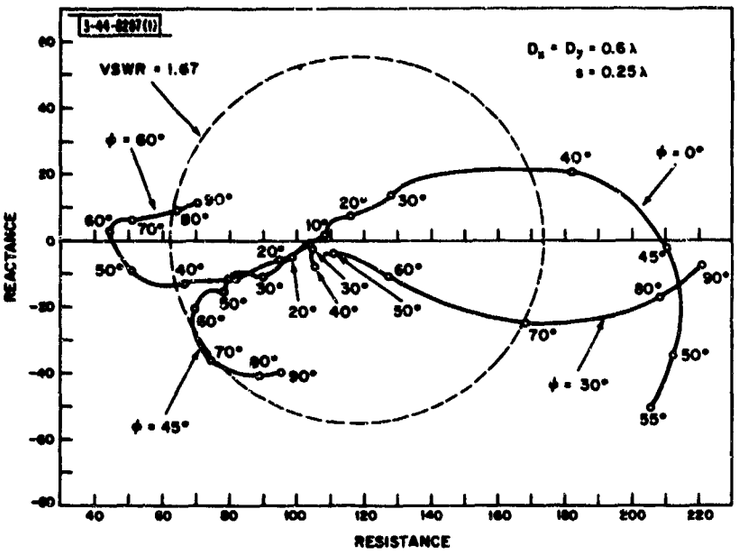

Fig. 39. Input port impedance variation for the center element of a 13 × 13 array of hybrid-fed, crossed-dipole pairs.

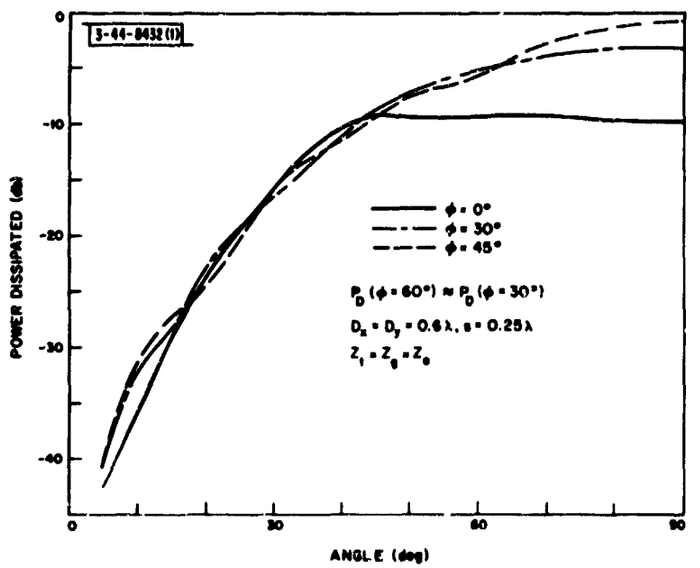

Fig. 40. Power dissipated in the orthogonal port termination for the center element of a 13 × 13 array of hybrid-fed, crossed-dipole pairs.

cross-polarized elements fed by a hybrid. In addition, the input impedance variation with scan angle at port 1 of Fig. 34 and the power dissipated (relative to the power available from the source) in the orthogonal port termination, as shown in Figs. 39 and 40, should be within approximately 10 percent of that which would be observed in a very large array.

From the above results, it is evident that mutual coupling effects can substantially alter the characteristics (gain, impedance, and polarization variation with scan angle) of a circularly polarized element when it is placed in an array environment. However, it is also clear that a properly designed array of hybrid-fed, crossed-dipole pairs will give good performance for moderate scan angles ($\Theta_{max} \approx 40°$). Observe that the characteristics of an element in an array depend on the array geometry for both linearly polarized and circularly polarized dipole arrays; for example, there is an optimum height above the ground plane for every inter-element spacing. It is also worth noting that the input impedance as seen by a source driving an element in an array varies somewhat less with scan angle for crossed-dipole arrays (compared to linearly polarized arrays), particularly in the reactive part.

It should be stressed that these results are dependent on the circuit used to obtain the two orthogonal excitations. For example, if the fourth port of the hybrid were left open-circuited, the power dissipated in that port when it is terminated (Fig. 40) would be reradiated instead of absorbed. Examination of the phases involved shows that such radiation is of the opposite sense circular polarization to that desired, resulting in greater depolarization than indicated by Figs. 36-38. In fact, it has been pointed out[19] that to minimize depolarization effects due to coupling in more than one polarization, it is necessary to provide a matched load to <u>all</u> polarizations, even if only one is desired. For example, in an array designed solely to radiate one sense of circular polarization, a load must be provided to the other sense to minimize depolarization.

4. Pattern Behavior of Irregular Arrays

The possibility of shaping the far-field patterns of arrays with equal amplitude excitation by unequally spacing the elements has been extensively studied, but almost exclusively under the assumption that the effect of the mutual coupling between the elements can be ignored.† There is experimental and theoretical evidence,[20] however, that the effect of coupling on the patterns of such arrays is not generally negligible. For example, Fig. 41 compares the pattern of an unequally spaced array of Galejs[21] as computed ignoring coupling, and as computed assuming the array to be constructed of parallel short dipoles 0.25 λ above ground, independently fed by sources of the type shown in Fig. 22, with Z_g chosen to match the impedance of an isolated dipole 0.25 λ above ground. The patterns shown are for a broadside beam; the relative pattern (most notably, the near-in sidelobe ratio) also varies with scan angle in the presence of coupling as indicated by the corresponding patterns of Fig. 42.

The necessity for including coupling in pattern computations for unequally spaced arrays is in marked contrast to the fact that the effects of coupling <u>can</u> safely be ignored in relative pattern computations for large <u>equally</u> spaced arrays. This latter simplification is, of course, due to the fact that for regular arrays large enough to ignore edge effects, all elements in the array "see" the same coupling environment and, hence, have the same input impedance.

There are only two cases in which it is certain that the effects of such coupling on the shape of the pattern are negligible. First, these effects can certainly be ignored when the elements

† See Ref. 21 for a recent bibliography.

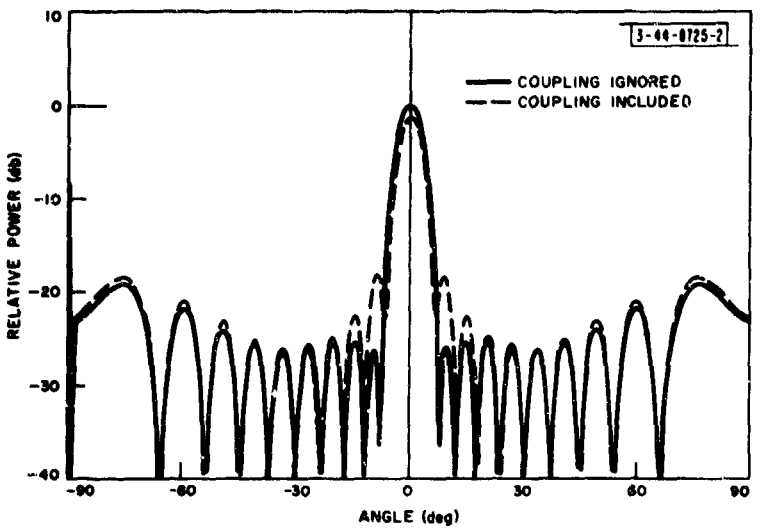

Fig. 41. Comparison of computed parallel dipole array factors for an unequally spaced array; broadside beam.

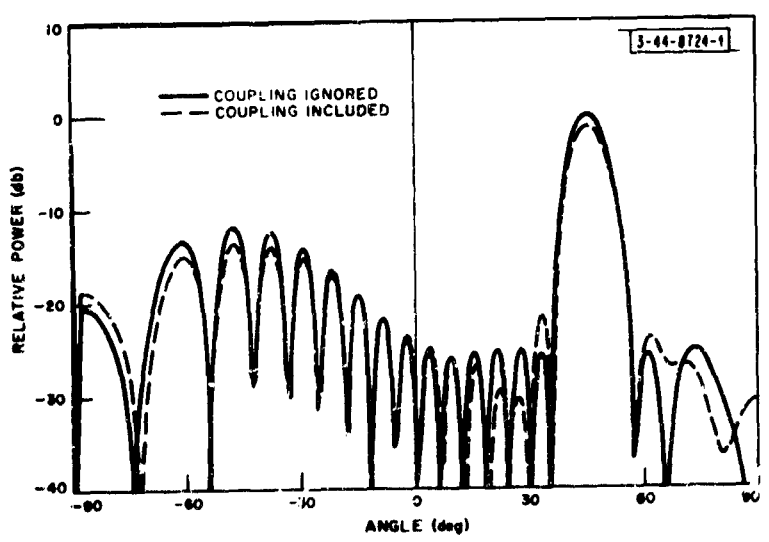

Fig. 42. Comparison of computed parallel dipole array factors for an unequally spaced array; 45° scan angle from broadside beam.

are fed by ideal constant-current generators so that their excitation is independent of their impedance. However, such generators are hard to find. Second, coupling can obviously be ignored when essentially all elements of an array are widely separated compared to the aperture area of such an element. This is not usually an acceptable solution in practical arrays, since unequal spacing allows control of the sidelobes commensurate with that of an equally spaced, amplitude tapered array only over a limited angle about the main beam. This region is out to an angle approximately equal to that at which a grating lobe would form for an equally spaced array with spacing equal to the average spacing $\bar{D}_n$ of an unequally spaced array; that is, to an angle ξ_1 from the main beam given by

$$1 + \sin|\xi_1| = \frac{1}{\bar{D}_n/\lambda} \quad . \tag{36}$$

Beyond this region, the sidelobes tend to be more or less random with an average relative sidelobe level given by the reciprocal of the number of elements. Thus, control over a sizeable fraction of visible space requires that the average spacing between the elements be less than a wavelength. For such spacing, coupling effects are certainly not negligible.

A practical model for the excitation circuit of a typical array of independently fed elements was indicated in Fig. 22. Since it is both desirable and common to attempt to control only the open-circuit voltages of the generators of such circuits (rather than the currents which depend on the mutual coupling), we will assume that these voltages have been chosen to be equal in magnitude and progressively phased for beam pointing; i.e., $e_n = e_o \exp[-jkz_n \sin\xi_o]$ for a desired pointing angle ξ_o, for elements located at points z_n along a line. In the absence of coupling, the array factor would then simply be proportional to

$$A(\xi) = \frac{e_o}{Z_g + Z_a} \sum_n \exp[jkz_n(\sin\xi - \sin\xi_o)] \quad . \tag{37}$$

We have seen in Fig. 41 that the agreement between the array factor as given by Eq. (37) and the array factor as computed for practical arrays including coupling is quite poor, particularly in the sidelobe region near the main beam. The reason is not hard to find.

As pointed out in Sec. III-B-2, the contribution of an element to the far field at any angle is proportional to the pattern of that element at that angle when the element is excited in the presence of the remainder of the elements, the latter passively terminated in Z_g. The shape of such patterns in equally spaced arrays depends markedly on the spacing between the element and its neighbor. Figure 43 shows the general behavior of the patterns of parallel dipoles 0.25 λ above ground in a linear array as a function of element spacing (the behavior of other elements in a linear array shows a similar trend). An approximate model for the dependence of the element gain function on the spacing between elements of a linear array† and the observation angle ξ is

$$|f(\xi)|^2 \approx \frac{D/\lambda}{1 + [D/\lambda(1 + |\sin\xi|)]} |f_e(\xi)|^2 \tag{38}$$

where [x] indicates the largest integer in x, and $|f_e(\xi)|^2$ is the power pattern of an isolated element. The denominator appears complicated, but merely represents the number of grating lobes

† For planar arrays, the variation is with the area allotted the elements rather than with the length. The following arguments are applicable to such arrays with this change in dependence.

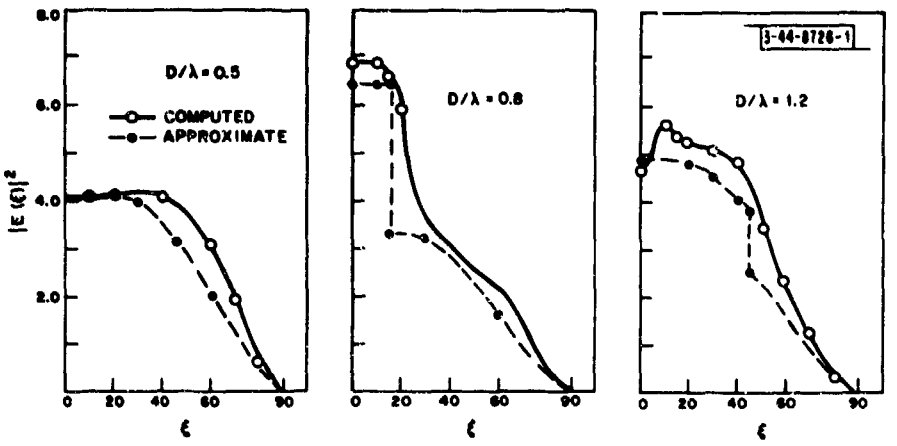

Fig. 43. Gain functions for elements in linear arrays with various inter-element spacings.

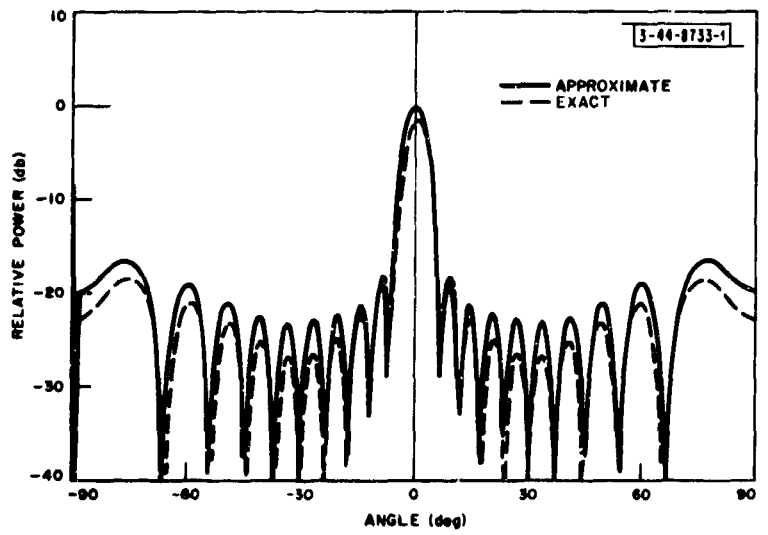

Fig. 44. Comparison of parallel dipole array patterns obtained using both exact and approximate methods for including coupling in an unequally spaced array.

in visible space for an array with spacing D and pointing angle ξ. Figure 43 compares this model with the accurately computed element patterns, and the agreement is generally good.

This agreement suggests that the patterns of unequally spaced arrays including coupling may be well approximated, if the change in spacing is a slowly varying function of position, by a similar function for the contribution of each element. Under this assumption, the array factor is given by

$$A(\xi) \propto \sum_n \left\{ \frac{D_n/\lambda}{1 + [D_n/\lambda(1 + |\sin\xi|)]} \right\}^{1/2} \exp[jkz_n(\sin\xi - \sin\xi_o)] \qquad (39)$$

where D_n is the spacing allotted the n^{th} element

$$D_n = \frac{z_{n+1} - z_{n-1}}{2} \quad .$$

In Fig. 44, we show an array pattern computed with the use of the approximation of Eq. (39) as compared with the computed parallel dipole array pattern of Fig. 41. The comparison with the curve of Fig. 41 that includes mutual coupling effects indicates that the approximation is quite good. A further simplification is suggested by the observation that the coupling principally affects the sidelobes near the main beam and has little effect on the far-out lobes. This suggests that substituting the pointing angle ξ_o in place of ξ in the denominator of Eq. (39) would be an acceptable approximation; i.e.,

$$A(\xi) \approx \sum_n \left\{ \frac{D_n/\lambda}{1 + [D_n/\lambda(1 + |\sin\xi_o|)]} \right\}^{1/2} \exp[jkz_n(\sin\xi - \sin\xi_o)] \quad . \qquad (40)$$

Array factors computed using Eq. (40) compare reasonably well with those computed using Eq. (39).

C. Coupling Effects in Arrays with Nonisolating Feeds

When a finite array is fed by a reactive network, several effects can occur in addition to the gain and impedance variations discussed above. In particular, there are problems associated with multiple reflections, phase shifter properties, resonance phenomena, and bandwidth. Some of these problems will be discussed in this section for both reactive corporate feeds and reactive series feeds. The corporate feed that we consider is constructed with three-port (reactive) junctions, as shown schematically in Fig. 45 for a 1:8 power divider.

The scattering matrix for a $1:2^K$ (=N) reactive corporate feed using 3-db junctions can be obtained by following a wave through the structure when only one port is excited with all others properly terminated. Part of such an incident wave will be reflected back to the driven port by the junctions, while the remainder will continue through the structure to the other ports. The amplitude and phase of a wave <u>out</u> of a particular port will then be the corresponding scattering coefficient when the input wave has unit amplitude and zero phase. For example, consider a unit wave incident on an output port of the 1:8 divider: at the first junction, half the incident wave will be reflected back to the driven port and will arrive with $(-2k\ell_1 - \pi)$ phase shift, and similarly for the other reflections. The wave returned to the driven port for this case can be shown to be

$$-\frac{1}{2} \exp[-j2k\ell_1] \left\{1 + \frac{1}{2} \exp[-j2k\ell_2] + \frac{1}{4} \exp[-j2k(\ell_2 + \ell_3)]\right\} \quad .$$

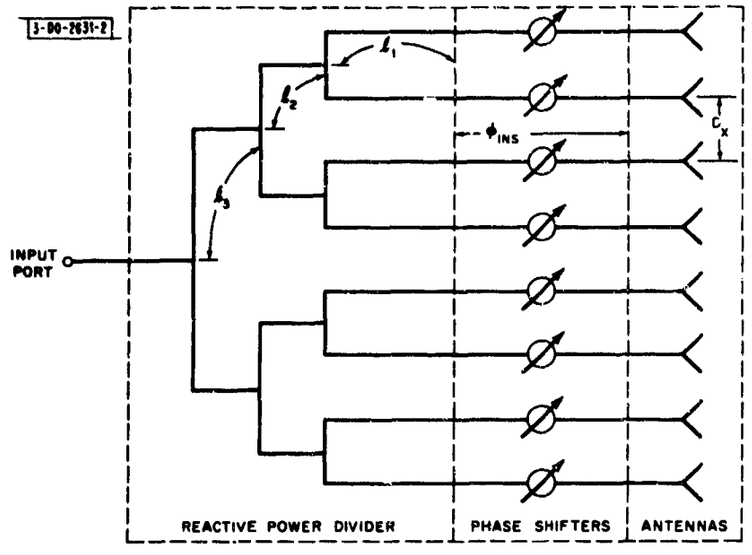

Fig. 45. Model for a 1:8 reactive corporate feed.

For the general case of a corporate feed with K levels of power division (1:2^K power divider), the self-scattering term at each output port S_o is

$$S_o = -\frac{1}{2} \exp[-j2k\ell_1] \left\{1 + \sum_{n=2}^{K} \frac{1}{2^{n-1}} \exp\left[-j2k \sum_{m=2}^{n} \ell_m\right]\right\} \quad . \tag{41}$$

The scattering coefficients for waves coupled from the driven output port to the other output ports are

$$S_{2n-1} = \frac{1}{2^n} \exp\left[-j2k \sum_{m=1}^{n} \ell_m\right] \left\{1 - \sum_{m=n+1}^{K} \frac{1}{2^{m-n}} \exp\left[-j2k \sum_{p=n+1}^{m} \ell_p\right]\right\} \tag{42}$$

where $2n - 1$ is the minimum number of junctions encountered in traversing the feed from the i^{th} output port to the j^{th} output port. (Note that n ranges from one to K, giving only K distinct cross-coupling terms. Also, for n = K, the summation term in brackets is zero.) This leaves just the <u>forward</u> coupling from the input port to each of the output ports:

$$S_f = 2^{-K/2} \exp\left[-jk \sum_{m=1}^{K} \ell_m\right] \quad . \tag{43}$$

It is readily evident from the above results that the scattering matrix for this type of feed is strongly dependent on the electrical lengths of the junctions. For example, the self-scattering term can vary in amplitude from a minimum value of $1/2^K$ (for $\ell_2 = \lambda/4$ and $\ell_n = \lambda/2$, $n > 2$) up to a maximum value of $1 - 1/2^K$ (for $\ell_n = \lambda/2$; $n \geq 2$). The other scattering coefficients have similar variations ranging from $1/2^K$ up to

$$|S_{2n-1}| = \frac{1}{2^{n-1}} - \frac{1}{2^K} \quad . \tag{44}$$

Also observe that

$$S_1 - S_o = \exp[-j2k\ell_1]$$

which means that minimum self-reflection occurs when the first-order cross-coupling is maximum and vice versa. These limiting values for the scattering coefficients indicate that the scattering matrix can vary substantially as the frequency is varied over a moderate range when practical line lengths are used. This indicates that there will be a bandwidth limitation to any practical corporate feed system.

With the feed scattering matrix thus defined, a relatively straightforward computation will solve for the overall performance of the antenna plus feed network system for a specified set of parameters. These computations, although conceptually quite simple, are very lengthy even with a high-speed digital computer because inversions of two large matrices are involved at each scan angle. For exact calculations, computer storage limits us to relatively small arrays ($\approx$ 64 elements); however, the approximate techniques discussed above can be successfully used to solve for the performance of a few elements in an array which is very large in one dimension.

For example, we have examined the behavior of the center row of 32 elements in a 32 × 65 dipole array driven by 65 identical, uncoupled,† reactive corporate feeds. When reciprocal phase shifters are used, reflection sidelobes can result as the beam is steered from broadside, as previously discussed. Figure 46 shows an example of these multiple reflection effects for a square-grid array with inter-element spacings of 0.6λ and mounted 0.25λ above a ground plane. Note that the reflection lobes in this case are very high because of relatively large antenna mismatches; for smaller angles of scan, the mismatches and, hence, the reflection lobes are decreased. If nonreciprocal phase shifters are used in this same array, the reflection lobes are essentially eliminated as indicated in Fig. 47.

We have also analyzed an 8 × 8 square-grid dipole array with each row of the array fed by a 1:8 reactive corporate feed. For this study, the array had an inter-element spacing of 0.6λ and no ground plane was used. An array of this size exhibits substantial edge effect when driven with independent sources; however, when properly designed reactive corporate feeds ($\ell_1 = \ell_2 = \ell_3 = 2.25\lambda$ in this case) are used, the currents in any row are constrained to have nearly identical amplitudes by the feed network as demonstrated by the top curve in Fig. 48.

This is a direct consequence of a property of lossless three-port junctions with output arm lengths an odd multiple of a quarter-wavelength long: the amplitudes of the currents in the two finite, nonzero loads terminating the output lines are in a constant ratio (unity for 3-db junctions) independent of the values of the loads. Unfortunately, this result only applies for a discrete set of line lengths and/or a discrete set of frequencies. For example, a 5-percent decrease in the operating frequency of the feed described above results in the array illumination shown in the bottom curve of the figure.

When this array is scanned by nonreciprocal phase shifters‡ to point a beam at $\Theta = 45°$, $\phi = 45°$, the current distribution across half the array at $f = 0.95\, f_o$ is as shown in the upper part of Fig. 49. The current distribution at broadside is also shown in the figure, from which it is readily seen that scanning the array to point a beam off broadside can substantially alter the array illumination. On the other hand, if the array is operated at the center frequency, this statement does not apply, as demonstrated by the dashed curve of Fig. 50.

† That is, the 65 reactive feeds can be considered as isolated from one another, as would be the case if each reactive feed were fed by its own source or by a well-matched hybrid corporate feed.

‡ The phase shifters were assumed to be digital with a smallest phase increment of 45°.

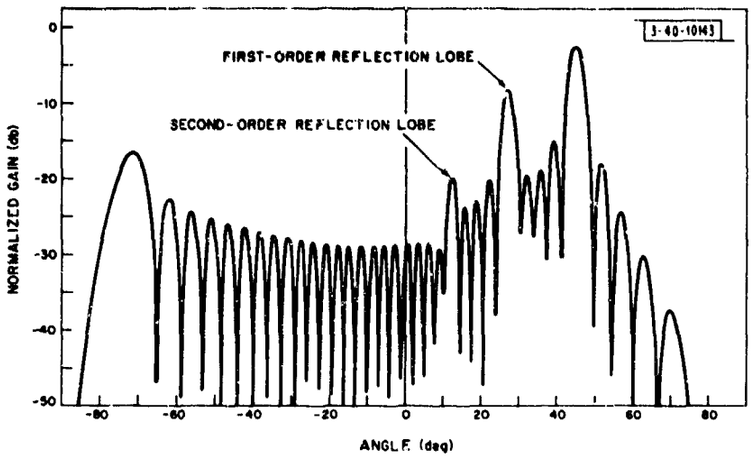

Fig. 46. Array pattern of a 32-element linear array fed by a reactive corporate feed network with reciprocal phase shifters.

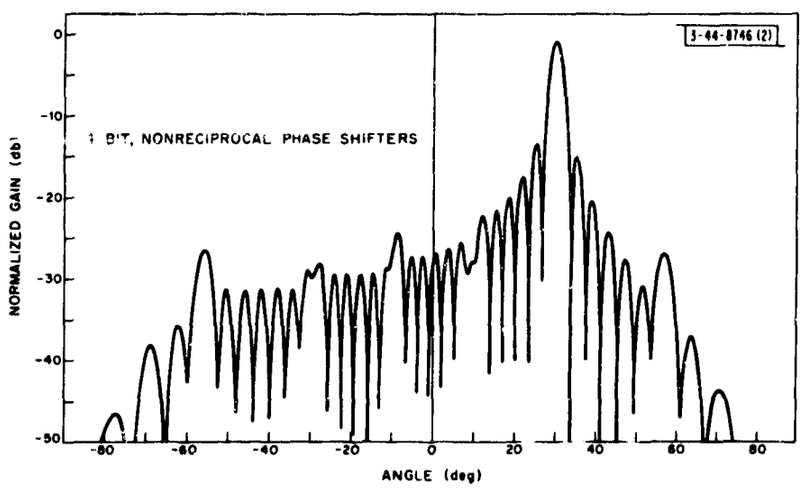

Fig. 47. Array pattern of a 32-element linear array fed by a reactive corporate feed network with nonreciprocal phase shifters.

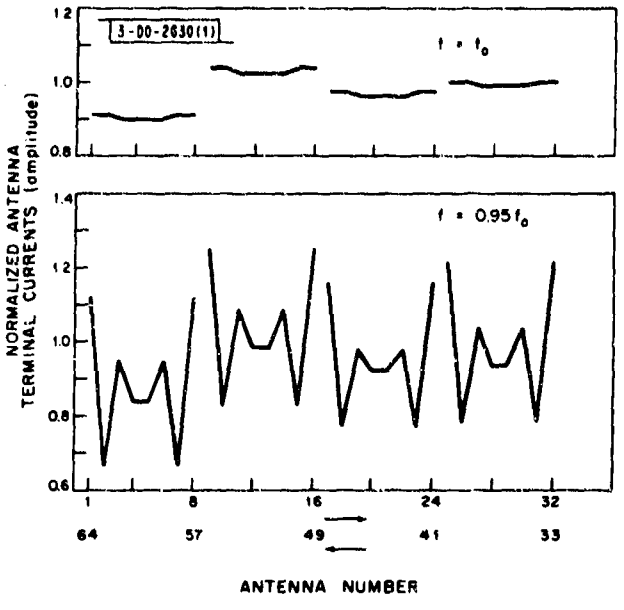

Fig. 48. Frequency dependence of the element currents in an 8 × 8 array fed by eight 1:8 reactive corporate feed networks.

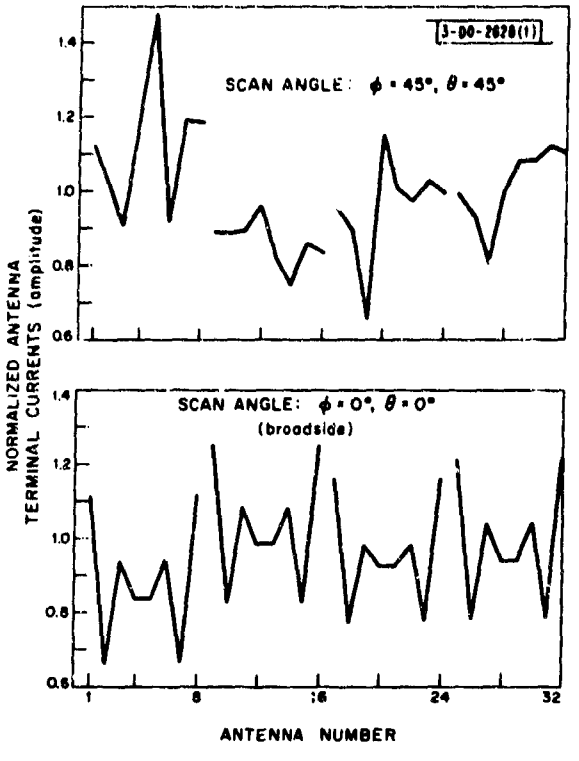

Fig. 49. Scan angle dependence of the element currents in an 8 × 8 array fed by eight 1:8 reactive corporate feed networks.

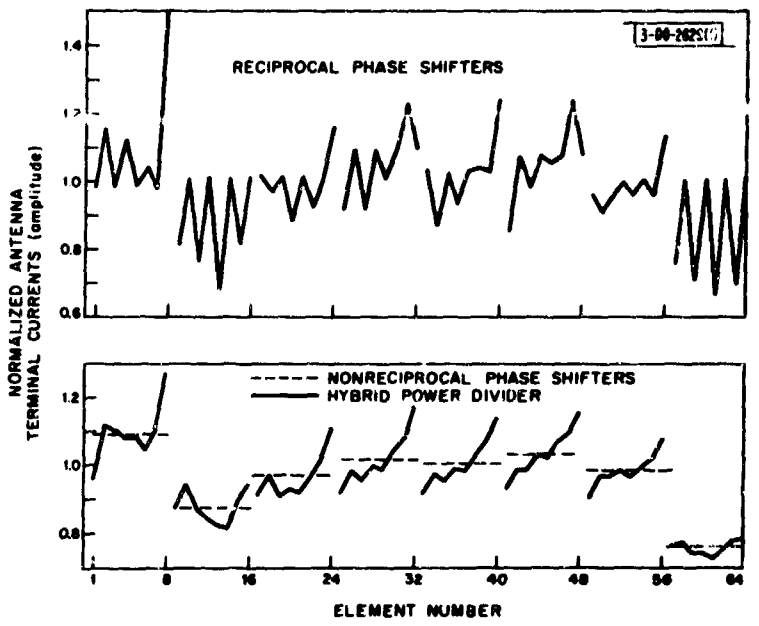

Fig. 50. Effect of feed network type and phase shifter type on the element currents in an 8 × 8 array.

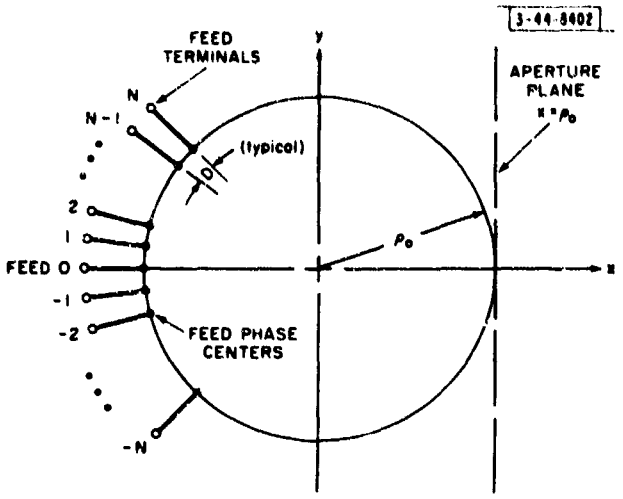

Fig. 51. Cylindrical beamforming lens geometry.

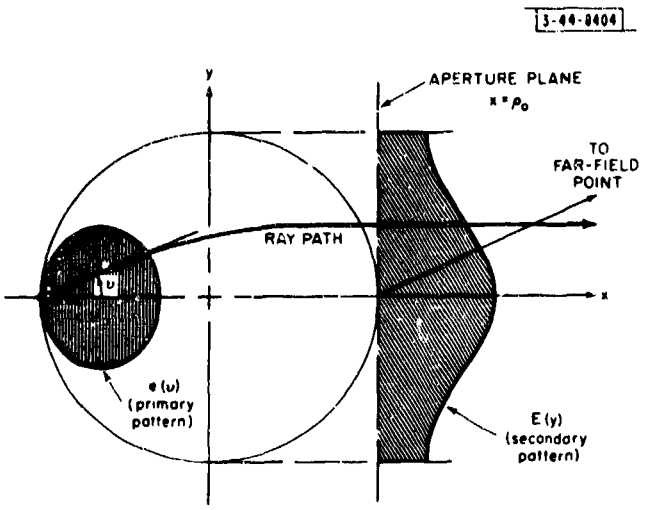

Fig. 52. Pattern nomenclature for a cylindrical beamforming lens.

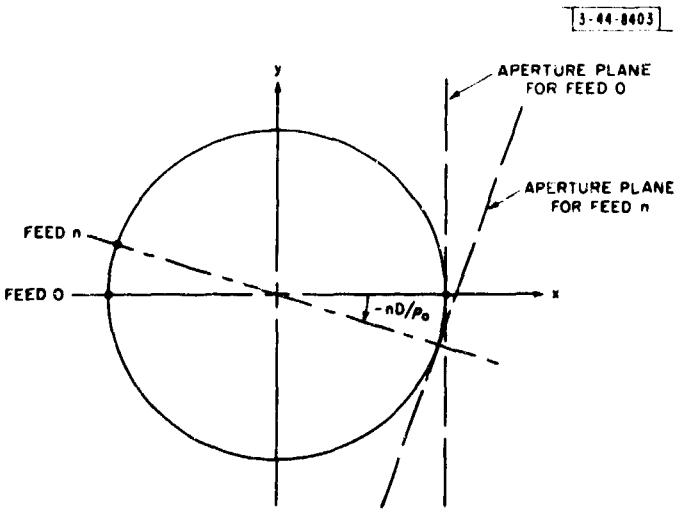

Fig. 53. Change in geometry with feed locations for a cylindrical beamforming lens.

This figure also shows the current distributions which result when analog reciprocal phase shifters and an independent (hybrid) source feed are used. Note that the use of reciprocal phase shifters results in a very poor array illumination taper and, as previously discussed, can cause very high reflection sidelobes when the beam is scanned off broadside. Also observe that reactive feed networks with nonreciprocal phase shifters can give an array illumination superior to that obtained with independent sources over a small band of frequencies.

IV. EFFECTS OF MUTUAL COUPLING ON RADIATION PATTERNS OF MULTIPLE-BEAM OPTICAL-TYPE ANTENNAS

There are several techniques for the realization of simultaneous multiple beams from antennas, with perhaps the oldest being the use of multiple feeds in conjunction with an optical-type antenna, such as a reflector or a lens. For example, Fig. 51 illustrates a two-dimensional version of such an antenna – a Luneburg lens fed by multiple sources.

The multiple-feed problem has a precise counterpart in the theory of large arrays, and knowledge about the effect of coupling on the performance of large linear and planar arrays can be applied directly and easily to this problem. To illustrate, let us analyze the two-dimensional (cylindrical) Luneburg lens system of Fig. 51 (i.e., the figure is assumed to extend to $z = \pm\infty$).

Consider the arrangement of Fig. 52. The lens is fed by a single feed which produces an electric field per unit current into the feed of $e(\nu)$, where ν is the angle measured from the phase center of the feed (we assume it has one). The lens performs a linear transformation on $e(\nu)$ to produce a secondary illumination $E(y)$.† For example, if the cylindrical lens is designed so that the feed phase centers are on the lens surface, geometrical optics will show that

$$E(y) = \frac{e(\nu)}{(\rho_o \cos\nu)^{1/2}} \quad , \quad y = \rho_o \sin\nu \quad . \tag{45}$$

The far field at a range R is then determined to within a phase factor by[22]

$$E(\xi) = \frac{1}{R\lambda} \int_{-\rho_o}^{\rho_o} E(y) \exp[jky \sin\xi]\, dy \tag{46}$$

where $k = 2\pi/\lambda$.

The actual form of the transformation is of little consequence to the argument, however. It suffices for now to use as a starting point the statement that energizing a single, isolated feed at a location corresponding to the n = 0 position of Fig. 51 produces an equiphase illumination along the aperture plane of $E_o(y)$ per unit feed current.

If the single feed is moved to a new position – say, the n^{th} of Fig. 51 – the aperture plane moves around the lens through an angle nD/ρ_o radians, as illustrated by Fig. 53. The phase front is tilted by nD/ρ_o radians relative to the y-axis, and the phase center of the aperture plane has moved from $x = R_o$, $y = 0$, to $x = \rho_o \cos nD/\rho_o$, $y = \rho_o \sin nD/\rho_o$. Obviously, if $nD/\rho_o \ll 1$, the displacement of the phase center in the x-direction becomes negligible, while the y displacement approaches nD. However, if $\rho_o \gg \lambda$, as assumed, most of the pattern structure of interest will lie near $\xi = 0$ of Fig. 52, and the y-offset of the phase center will have little effect on close-in sidelobe levels.

† The dimensions on $e(\nu)$ and $E(y)$ differ, so that squaring each and dividing by the intrinsic impedance of free space produces watts per unit solid angle and watts per unit surface area, respectively.

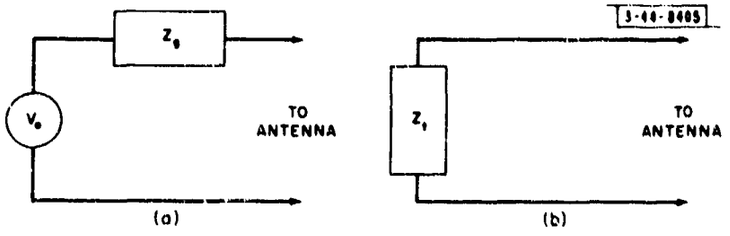

Fig. 54. Assumed feed circuit configurations for a cylindrical beamforming lens.

As a result of the foregoing approximations, the change in the aperture illumination on a line parallel to the y-axis that results from moving the feed appears as simply a change in phase front slope

$$E_n(y) = E_o(y) \exp\left[jkn \frac{Dy}{\rho_o}\right] \tag{47}$$

when viewed at small angles from broadside.

Returning to the multiple-feed configuration of Fig. 51, if we excite feed 0 with, for example, a voltage generator of open-circuit voltage V_o as in Fig. 54(a), and terminate the other feeds as in Fig. 54(b), then the current in the n^{th} feed is just

$$I_n = V_o Y_{no} \tag{48}$$

where Y_{no} is the mutual admittance between feeds n and 0 (a function of the feed types, feed placements, and Z_g and Z_t of Fig. 54). The total illumination along a line parallel to the y-axis $E_t(y)$ is then

$$E_t(y) = \sum_{n=-N}^{N} I_n E_n(y)$$

which, by Eqs. (47) and (48), gives†

$$E_t(y) = E_o(y)\, V_o \sum_{n=-N}^{N} Y_{no} \exp\left[jknD \frac{y}{R_o}\right] \quad . \tag{49}$$

Thus for a large ($\rho_o >> \lambda$) optical system, the far field in the region near the main beam will be the Fourier transform of Eq. (49), where $E_o(y)$ is the aperture illumination per unit current into the feed that would result from a single feed placed on the x-axis.

Equation (49) can be put explicitly in the form of the primary feed illumination. The effect of the optical system on a single point source feed is to transform the feed primary pattern – say, $e_o(\nu)$, where ν is the angle from the x-axis as indicated in Fig. 52 – into $E_o(y)$ by some linear transformation, which we will denote as an operation L.

$$E(y) = L\, e(\nu) \quad . \tag{50}$$

For example, for a surface-focused Luneburg lens, the transformation is given by Eq. (45). The exact form of the transformation is not of immediate consequence here, only the fact that it is

† The purist may object to the implicit assumption that the pattern which results from a feed being driven at its terminals and the same feed being parasitically excited is necessarily the same. This assumption, which was used to simplify notation, is not really necessary to the argument.

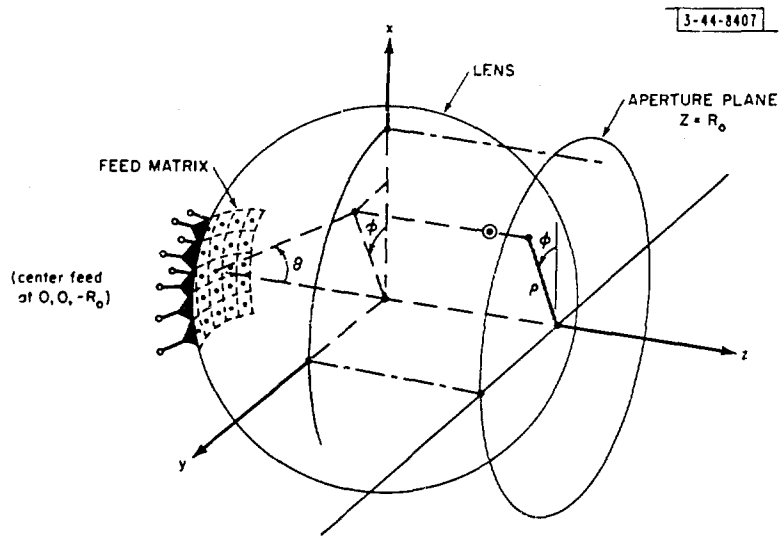

Fig. 55. Spherical beamforming lens geometry.

linear, which allows us to transform both sides of Eq. (49) to give

$$e_t(\nu) = e_o(\nu)\, V_o \sum_{n=-N}^{N} Y_{no} \exp[jknD \sin\nu] \tag{51}$$

where we have used $y = \rho_c \sin\nu$ in the exponent as appropriate to the Luneburg lens, since the phase slope in Eqs. (47) and (49) was derived for this configuration.

The physical interpretation of $e_t(\nu)$ is that $e_o(\nu)$ of Eq. (51) is the pattern of one element of a linear array taken in the presence of the remainder of the elements when they are passively terminated, i.e., the "element pattern" of Sec. III-B, if there are enough feeds on either side of the element in question to assume an infinite number. The results are directly applicable to three-dimensional optical feeds as in Fig. 55, with the planar array gain function used for feeds arrayed as in the figure.

> Thus the conclusion of the analysis is that a multiple feed in an optical system will radiate a pattern whose shape close to the main beam is given by transforming the pattern of one feed in the presence of the other feeds when they are terminated in the impedance normally used.

This conclusion is based on the following approximations:

(a) $\rho_o \gg \lambda$, and therefore geometrical optics is valid.

(b) The lens is large enough so that the feed assembly (or the extent of the feed over which elements couple appreciably) is small enough for the curvature to be negligible.

(c) The array is large enough so that the main beam and sidelobe region of interest is of small angular extent, since for angles very far from the line through the excited feed (the x-axis of Fig. 51 if feed 0 is excited), the difference in phase center locations of the aperture planes for the various feeds is not negligible in the direction of interest.

In substance, these approximations amount to a restriction to very large (narrow-beam) systems.

REFERENCES

1. P.W. Hannan, "The Element-Gain Paradox for a Phased-Array Antenna," Trans. IEEE, PTGAP AP-12, 423 (1964).
2. P.W. Hannan, "A Proof That a Phased Array Antenna Can Be Impedance Matched for All Scan Angles," Radio Sci. (JNBS), to be published.
3. J. L. Allen, et al., "Phased Array Radar Studies, 1 January 1963 to 1 July 1964," Technical Report 381, Lincoln Laboratory, M. I. T. (31 March 1965), pp. 299-318, DDC 629363.
4. W. E. Rupp, "Antenna Mutual Impedance Bridge," Microwave J. 5, 95 (August 1962).
5. P.W. Hannan and M.A. Balfour, "Simulation of a Phased-Array Antenna in a Waveguide," IEEE Trans. Antennas Propag. AP-13, 342 (1965).
6. J. L. Allen, "The Theory of Array Antennas (with Emphasis on Radar Applications)," Technical Report 323, Lincoln Laboratory, M. I. T. (25 July 1963), DDC 422945, H-563.
7. H.A. Wheeler, "Simple Relations Derived from a Phased-Array Antenna Made of an Infinite Current Sheet," IEEE Trans. Antennas Propag. AP-13, 506 (1965).
8. H.A. Wheeler, "The Radiation Resistance of an Antenna in an Infinite Array or Waveguide," Proc. IRE 36, 478 (1948).
9. S. Edelberg and A.A. Oliner, "Mutual Coupling Effects in Large Antenna Arrays (Parts I and II)," Trans. IRE, PGAP AP-8, 286 and 360 (May and July 1960).
10. L. Stark, "Radiation Impedance of a Dipole in an Infinite Planar Phased Array," Radio Sci. (JNBS) 1 (new series), 361 (1966).
11. H.A. Wheeler, "The Grating-Lobe Series for the Impedance Variation in a Planar Phased-Array Antenna," IEEE Trans. Antennas Propag. AP-13, 825 (1965).
12. L. Parad, "The Real and Reactive Power of a Planar Array," IEEE Trans. Antennas Propag. AP-13, 890 (1965).
13. D.R. Rhodes, "On a Fundamental Principle in the Theory of Planar Antennas," Proc. IEEE 52, 9 (1964).
14. B. L. Diamond and T.B. Lewis, "Correlation of Experimental and Theoretical Active Impedances of a Dipole in an Array," IEEE Trans. Antennas Propag. AP-13, 806 (1965), DDC 627136.
15. J.D. Kraus, Antennas (McGraw-Hill, New York, 1950).
16. L.A. Kurtz and R.S. Elliot, "Systematic Errors Caused by the Scanning of Antenna Arrays: Phase Shifters in the Branch Lines," Technical Memo 359, Hughes Aircraft Company, Culver City, California (1 May 1953).
17. Ref. 3, pp. 239-298.
18. Ref. 6, p. 61.
19. L. I. Parad and R.W. Kreutel, "Mutual Effects Between Circularly Polarized Elements," Antenna Arrays Section of the Abstracts on the Twelfth Annual Symposium, USAF Antenna Research and Development Program, University of Illinois (October 1962).
20. J. L. Allen and W. P. Delaney, "On the Effect of Mutual Coupling on Unequally Spaced Dipole Arrays," Trans. IRE, PGAP AP-10, 784 (1962).
21. J. Galejs, "Minimization of Sidelobes in Space Tapered Linear Arrays," Trans. IEEE, PTGAP AP-12, 497 (1964).
22. S. Silver, Microwave Antenna Theory and Design, Radiation Laboratory Series, M. I. T. (McGraw-Hill, New York, 1949), Vol. 12, p. 173.

DOCUMENT CONTROL DATA – R&D

(Security classification of title, body of abstract and indexing annotation must be entered when the overall report is classified)

1. ORIGINATING ACTIVITY *(Corporate author)*
Lincoln Laboratory, M.I.T.

2a. REPORT SECURITY CLASSIFICATION
Unclassified

2b. GROUP
None

3. REPORT TITLE
Mutual Coupling in Array Antennas

4. DESCRIPTIVE NOTES *(Type of report and inclusive dates)*
Technical Report

5. AUTHOR(S) *(Last name, first name, initial)*
Allen, John L. and Diamond, Bliss L.

6. REPORT DATE	7a. TOTAL NO. OF PAGES	7b. NO. OF REFS
4 October 1966	68	23

8a. CONTRACT OR GRANT NO.	9a. ORIGINATOR'S REPORT NUMBER(S)
AF 19(628)-5167	Technical Report 424
b. PROJECT NO. ARPA Order 498	9b. OTHER REPORT NO(S) *(Any other numbers that may be assigned this report)* ESD-TR-66-443
c.	
d.	

10. AVAILABILITY/LIMITATION NOTICES
Distribution of this document is unlimited.

11. SUPPLEMENTARY NOTES	12. SPONSORING MILITARY ACTIVITY
None	Advanced Research Projects Agency, Department of Defense

13. ABSTRACT

The report summarizes the current level of understanding of the performance of arrays of real radiators. The extent and nature of the effects of mutual coupling (element pattern distortion, element impedance variation with scan angle, and polarization variation with scan angle) in array antennas are investigated for a variety of array geometries and for several types of radiating elements. Both finite and infinite arrays of regularly spaced, uniformly illuminated, and progressively phased elements are considered. The effects of coupling on unequally spaced arrays, arrays with coupled feed networks, and circularly polarized arrays are also discussed. Finally, the results of a study of the effects of coupling on the radiation patterns of multiple-beam optical-type antennas are presented. Although most of the numerical results are based on thin-dipole radiating elements with and without ground planes (the dipole without a ground plane is the exact dual of an array of slots in a ground plane), both theoretical and experimental investigations of the sensitivity of the results to the element type are included. Emphasis is placed on the results of various analyses and their implications to the array designer. The derivations of some of the more important results are briefly outlined, but in most instances, only the relevant conclusions are given.

14. KEY WORDS

array antennas
antenna design
grating-lobe series
mutual coupling
dipole arrays
crossed-dipole arrays
unequally spaced arrays
optical-type beamforming